Chapter 4

Perovskite Nanomaterials – Synthesis, Characterization, and Applications

Nada F. Atta, Ahmed Galal and Ekram H. El-Ads

Additional information is available at the end of the chapter

http://dx.doi.org/10.5772/61280

Abstract

Inorganic perovskite-type oxides are fascinating nanomaterials for wide applications in catalysis, fuel cells, and electrochemical sensing. Perovskites prepared in the nanoscale have recently received extensive attention due to their catalytic nature when used as electrode modifiers. The catalytic activity of these oxides is higher than that of many transition metals compounds and even some precious metal oxides. They exhibit attractive physical and chemical characteristics such as electronic conductivity, electrically active structure, the oxide ions mobility through the crystal lattice, variations on the content of the oxygen, thermal and chemical stability, and super-magnetic, photocatalytic, thermoelectric, and dielectric properties.

Nanoperovskites have been utilized as catalysts in oxygen reduction and hydrogen evolution reactions exhibiting high electrocatalytic activity, lower activation energy, and high electron transfer kinetics. In addition, some perovskites are promising candidates for the development of effective anodic catalysts for direct fuel cells showing high catalytic performance. Moreover, they are recently utilized in electrochemical sensing of alcohols, gases, glucose, H_2O_2, and neurotransmitters. They can enhance the catalytic performance in terms of selectivity, sensitivity, unique long-term stability, excellent reproducibility, and anti-interference ability. In addition, organometallic halide perovskites exhibited efficient intrinsic properties for photovoltaic solar cells exhibiting good stability and high efficiency.

This chapter introduces a comprehensive coverage of the progress in perovskites research and their applications. Emphasis is given toward several intrinsic properties of perovskites, namely, electronic conductivity, electrically active structure, and electrochemical performance in terms of synthesis routes and stability. The different synthesis methods of the perovskites (coprecipitation, sol-gel, microwave, citrate/nitrate, etc.) will be summarized in this chapter. The synthesis method affected

structural, surface, and catalytic properties of the prepared perovskites to a great extent. Also, this chapter will update the reader with the various applications of nanoperovskites particularly in fuel cells, catalysis, electrochemical sensing, and solar cells.

Keywords: Nanomaterials, Perovskites, Sensors, Catalysis, Fuel cells

1. Introduction

1.1. General introduction to perovskites

The mineral $CaTiO_3$ was discovered by Geologist Gustav Rose in the Ural Mountains in 1839, and it was named perovskite in recognition beholden to Count Lev Alexevich von Perovski, an eminent Russian mineralogist [1–5]. The name perovskite represented any compound that has ABC_3 formula where an octahedron of C ions surrounded the B ion. The Earth's crust contains various types of perovskites and the most abundant ones are $MgSiO_3$ and $FeSiO_3$. Perovskite family includes several types of oxides like transition metal oxides with the formula ABO_3. Some examples of ABO_3 perovskites and their corresponding properties are summarized in Table 1 [1, 2, 5].

Perovskite oxides exhibit an array of electrical properties and a variety of solid-state phenomena from insulating, semiconducting, metallic, and superconducting characters; therefore, they are very fascinating to be studied and applied in a large scale. Many of ABO_3 perovskites are cubic or nearly cubic in structure in their ideal form; however, one or more phase transitions may be achieved particularly at low temperature. In addition, many of them showed magnetic ordering and as a result, large variety of magnetic structures can be found. Some perovskites contained localized electrons, some contained delocalized energy-band states, and the behavior of other perovskites was a transition between these two types. The perovskite structures can incorporate ions of various size and charge showing great flexibility of composition. Moreover, substitutions of ions into the A- and/or B-sites or deviation from ideal stoichiometry resulted in altering the electronic properties of the perovskites. Perovskites exhibit atomic arrangement in the form of 3-dimensional array of corner sharing octahedra. On the other hand, layered perovskites included 2-dimensional layers of corner sharing octahedral separated by cations layers. As a result, the electronic energy bands of perovskites and layered perovskites are very unusual and their structure is unique in properties [1, 2]. Perovskites displayed diversity of electric, optical, and magnetic properties because of the fact that 90% of the elements in the periodic table can be stable in the perovskite structure and the feasibility of partial substitutions of cations in A- and B-sites forming $A_{1-x}A'_xB_{1-y}B'_yO_3$ [6]. Perovskites showed great interest in several applications due to their wide various and useful properties in photochromic, electrochromic, image storage, switching, filtering, and surface acoustic wave signal processing devices. They were utilized as catalytically active catalyst for several reactions like carbon monoxide and hydrocarbons oxidation, hydrogen evolution

http://dx.doi.org/10.5772/61280

reaction and nitrogen oxides, and oxygen reduction reactions. They also have a good impact in many electrochemical applications like sensing, biosensing, photoelectrolysis of water-producing hydrogen, and fuel cells [1, 2].

Insulating	Metallic	Magnetic	Superconducting
			$SrTiO_3$ (n-type)
WO_3	ReO_3	$PbCrO_3$	Na_xWO_3 (t)
$NaTaO_3$	$NaWO_3$	$LaCrO_3$	K_xWO_3 (t)
$SrTiO_3$	$KMoO_3$	$CaMnO_3$	K_xWO_3 (h)
$BaTiO_3$	$SrNbO_3$	$LaMnO_3$	Rb_xWO_3 (h)
$KTaO_3$	$LaTiO_3$	$LaCoO_3$	Cs_xWO_3 (h)
$LiNbO_3$	$LaWO_3$	$LaFeO_3$	Li_xWO_3 (h)

t; tetragonal, h; hexagonal

Table 1. Some perovskites and corresponding properties [1].

1.2. Crystallography of the perovskite structure

In the ABO_3 form, B is a transition metal ion with small radius, larger A ion is an alkali earth metals or lanthanides with larger radius, and O is the oxygen ion with the ratio of 1:1:3. In the cubic unit cell of ABO_3 perovskite, atom A is located at the body center, atom B is located at the cube corner position, and oxygen atoms are located at face-centered positions (Figure 1). The 6-fold coordination of B cation (octahedron) and the 12-fold coordination of the A cation resulted in the stabilization of the perovskite structure. The perfect perovskite structure was described by Hines et al. as corner linked BO_6 octahedra with interstitial A cations [1–10]. Some distortions may exist in the ideal cubic form of perovskite resulted in orthorhombic, rhombohedral, hexagonal, and tetragonal forms (Figure 1) [3–7]. Figure 2 represented the distortion from cubic perovskite to orthorhombic one. In general, all perovskite distortions maintaining the A- and the B-site oxygen coordination was achieved by the tilting of the BO_6 octahedra and an associated displacement of the A cation [4].

V.M. Goldschmidt presented much of the early work on the synthetic perovskites and developed the principle of the tolerance factor *t*, which is applicable to the empirical ionic radii at room temperature [2–9]:

$$t = \left(r_A + r_O\right) \; / \; \left[2^{1/2}\left(r_B + r_O\right)\right],$$

where r_A is the radius of the A-site cation, r_B is the radius of the B-site cation, and r_O is the radius of oxygen ion O^{2-}. The tolerance factor can be used to estimate the suitability of the combination of cations for the perovskite structure [2]. It is a real measure of the degree of the distortion of

perovskite from the ideal cubic structure so the value of t tends to unity as the structure approaches the cubic form [4]. From the equation, the tolerance factor will decrease when r_A decreases and/or r_B increases. Based on the analysis of tolerance factor value, Hines et al. solely suggested that the perovskite structure can be estimated. For $1.00 < t < 1.13$, $0.9 < t < 1.0$, and $0.75 < t < 0.9$, the perovskite structure is hexagonal, cubic, and orthorhombic, respectively. For $t < 0.75$, the structure was adopted to hexagonal ilmenite structure ($FeTiO_3$) [4].

Generally, two requirements should be fulfilled for perovskite formation:

1. Electroneutrality; the perovskite formula must have neutral balanced charge therefore the product of the addition of the charges of A and B ions should be equivalent to the whole charge of the oxygen ions. An appropriate charge distribution should be attained in the forms of $A^{1+}B^{5+}O_3$, $A^{4+}B^{2+}O_3$ or $A^{3+}B^{3+}O_3$.

2. Ionic radii requirements; $r_A > 0.090$ nm and $r_B > 0.051$ nm, and the tolerance factor must have values within the range $0.8 < t < 1.0$ [2–8].

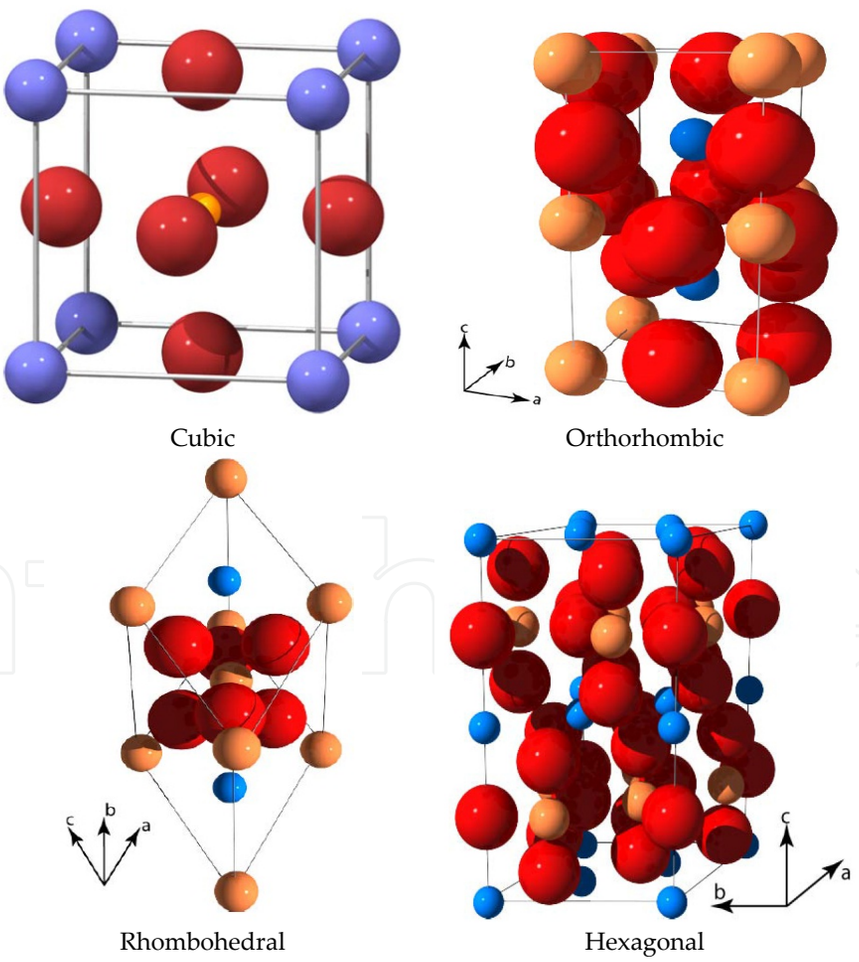

Figure 1. Different perovskite unit cells. Blue spheres represent the A cations, yellow spheres represent the B cations and red spheres represent oxygen anions forming an octahedra [4].

http://dx.doi.org/10.5772/61280

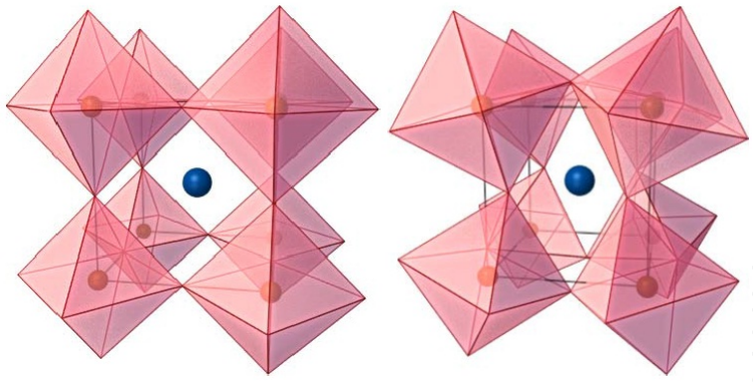

(a) cubic (b) orthorhombic

Figure 2. Perovskite distortion from (a) cubic to (b) orthorhombic [4].

1.3. Typical properties of perovskites

Perovskite exhibited a variety of fascinating properties like ferroelectricity as in case of $BaTiO_3$ and superconductivity as in case of $Ba_2YCu_3O_7$. They exhibited good electrical conductivity close to metals, ionic conductivity and mixed ionic and electronic conductivity. In addition, several perovskites exhibited high catalytic activity toward various reactions. Table 2 contains a summary of typical properties of perovskites. Several typical properties will be discussed in this section like ferroelectricity, magnetism, superconductivity, and catalytic activity [9].

Typical property	Typical compound
Ferromagnetic property	$BaTiO_3$, $PdTiO_3$
Piezoelectricity	$Pb(Zr, Ti)O_3$, $(Bi, Na)TiO_3$
Electrical conductivity	ReO_3, $SrFeO_3$, $LaCoO_3$, $LaNiO_3$, $LaCrO_3$
Superconductivity	$La_{0.9}Sr_{0.1}CuO_3$, $YBa_2Cu_3O_7$, $HgBa_2Ca_2Cu_2O_8$
Ion conductivity	$La(Ca)AlO_3$, $CaTiO_3$, $La(Sr)Ga(Mg)O_3$, $BaZrO_3$, $SrZrO_3$, $BaCeO_3$
Magnetic property	$LaMnO_3$, $LaFeO_3$, La_2NiMnO_6
Catalytic property	$LaCoO_3$, $LaMnO_3$, $BaCuO_3$
Electrode	$La_{0.6}Sr_{0.4}CoO_3$, $La_{0.8}Ca_{0.2}MnO_3$

Table 2. Typical properties of perovskite oxides [9].

1.3.1. Dielectric properties

There are some properties inherent to dielectric materials like ferroelectricity, piezoelectricity, electrostriction, and pyroelectricity. One of the important characteristic of perovskites is ferroelectric behavior, which is obvious in $BaTiO_3$, $PdZrO_3$, and their doped compounds. The ferroelectric behavior of $BaTiO_3$ was strongly related to its crystal structure. $BaTiO_3$ was

subjected to three phase transitions; as the temperature increases, it was converted from monoclinic to tetragonal then to cubic. At temperature higher than 303 K, $BaTiO_3$ does not show any ferroelectric behavior as it crystallizes into cubic structure. $BaTiO_3$ showed high dielectric constant based on the anisotropy of its crystal structure resulting in large dipole moment generation in $BaTiO_3$ [9].

1.3.2. Electrical conductivity and superconductivity

One of the obvious properties of perovskites is superconductivity. Cu-based perovskites act as high-temperature superconductors, and La-Ba-Cu-O perovskite was first reported. The presence of Cu in B-site is essential for the superconductivity and various superconducting oxides can be manufactured with different A-site ions. Some examples of high temperature superconductors are $YBa_2Cu_3O_7$, $Bi_2Sr_2Ca_2Cu_3O_{10}$, and $HgBa_2Ca_2Cu_3O_{8+\delta}$ with critical temperature of superconducting transition (Tc) of 130–155 K. The superconductivity is associated with the layers of Cu-O in Cu-based perovskites, and the Tc value is associated with the Cu-O layers number in the crystal lattice. The synthesis of 5 or more Cu-O-layered perovskites did not achieve successfully due to the low chemical stability. One of the highly significant superconductors with great Tc value is $YBa_2Cu_3O_7$. In addition, the oxygen nonstiochiometry is one of the most significant reasons for the high value of Tc. In $YBa_2Cu_3O_{7-\delta}$, when the value of $\delta < 0.5$, it crystallizes into orthorhombic structure, which is superconductive. For $\delta > 0.5$, it showed a tetragonal structure that does not show any superconductivity. The crystal structure affected greatly the superconductivity in high Tc oxides, and as a result, high Tc values can be achieved by improving the chemical stability of the perovskite crystal structure. Furthermore, some perovskites exhibited great electronic conductivity similar to that of metals like Cu. $LaCoO_3$ and $LaMnO_3$ are examples of perovskites exhibiting high electronic conductivity, and therefore they are utilized as cathodes in solid oxide fuel cells displaying superior hole conductivity of 100 S/cm. The electronic conductivity of the perovskites can be enhanced by doping the A-site with another cation, which resulted in increasing the quantity of the mobile charge carriers created by the reparations of charge [9].

1.3.3. Catalytic activity

Perovskites showed excellent catalytic activity and high chemical stability; therefore, they were studied in a wide range in the catalysis of different reactions. Perovskites can be described as a model of active sites and as an oxidation or oxygen-activated catalyst. The stability of the perovskite structure allowed the compounds preparation from elements with unusual valence states or a high extent of oxygen deficiency. Perovskites exhibited high catalytic activity, which is partially associated with the high surface activity to oxygen reduction ratio or oxygen activation that resulted from the large number of oxygen vacancies. Perovskites can act as automobile exhaust gas catalyst, intelligent automobile catalyst and cleaning catalyst, etc., for various catalytic environmental reactions. It was reported in the literature that perovskites containing Cu, Co, Mn, or Fe showed excellent catalytic activity toward the direct decomposition of NO at high temperature, which is considered one of the difficult reactions in the catalysis ($2NO \rightarrow N_2+O_2$). Perovskites showed superior activity for this reaction at high

http://dx.doi.org/10.5772/61280

temperatures because of the presence of oxygen deficiency and the simple elimination of the surface oxygen in the form of a reaction product. NO decomposition activity was enhanced upon doping. Also, under an atmosphere that is rich with oxygen up to 5%, Ba(La)Mn(Mg)O_3 perovskite exhibited superior activity toward the decomposition of NO [9].

Perovskite showed a great impact as an automobile catalyst; intelligent catalyst. Pd-Rh-Pt catalysts was utilized as an effective catalyst for the removal of NO, CO and uncombusted hydrocarbons. There is another catalyst that consists of fine particles, with high surface-to-volume ratio, and can be utilized to reduce the amount of precious metals used. However, these fine particles exhibited very bad stability under the operation conditions leading to catalyst deactivation. Therefore, perovskite oxides can be used showing redox properties to preserve a great dispersion state. Upon oxidation, Pd is oxidized in the form of $LaFe_{0.57}Co_{0.38}Pd_{0.05}O_3$ and upon reduction; fine metallic particles of Pd were produced with radius of 1–3 nm. This cycle resulted in partial replacement of Pd into and sedimentation from the framework of the perovskite under oxidizing and reducing conditions, respectively, displaying a great dispersion state of Pd. Also, this cycle improved the excellent long-term stability of Pd during the pollutants removal from the exhaust gas. Exposing the catalyst to oxidizing and reducing atmosphere resulted in the recovery of the high dispersion state of Pd. This catalyst is known as intelligent catalyst because of the great dispersion state of Pd and the excellent stability of the perovskite structure [9].

2. Methods of perovskite synthesis

2.1. Solid-state reactions

In solid-state reactions, the raw materials and the final products are in the solid-state therefore nitrates, carbonates, oxides, and others can be mixed with the stoichiometric ratios. Perovskites can be synthesized via solid-state reactions by mixing carbonates or oxides of the A- and B-site metal ions corresponding to the perovskite formula ABO_3 in the required proportion to obtain the final product with the desired composition. They are ball milling effectively in an appropriate milling media of acetone or isopropanol [11, 12]. Then the obtained product is dried at 100 °C and calcined in air at 600 °C for 4–8 h under heating/cooling rates of 2 °C/min. After that, the calcined samples are ground well and sieved. Then it was calcined again at 1300–1600 °C for 5–15 h under the heating/cooling rate of 2 °C/min to confirm the formation of single phase of perovskite. Again grinding and sieving was carried out for the calcined samples [11, 13, 14]. The synthesis of $BaCeO_3$-based proton conductor perovskites [13] and $BaCe_{0.95}Yb_{0.05}O_{3-\delta}$ [11] was achieved through the previous methodology using $BaCO_3$, CeO_2, and Yb_2O_3 as the starting materials and isopropanol as the milling media [10].

2.2. Gas phase preparations

Gas phase reaction or transport can be used for the deposition of perovskite films with a specific thickness and composition. Laser ablation [15], molecular beam epitaxy [16], dc sputtering [17], magnetron sputtering [18], electron beam evaporation [19], and thermal evaporation [20]

techniques were developed for gas phase deposition. Gas phase deposition can be categorized into three types: (i) deposition at a low substrate temperature then postannealing at high temperature, (ii) deposition at an intermediate temperature of 873 to 1,073 K then postannealing treatment, and (iii) deposition at the crystallization temperature under suitable atmosphere. $YBa_2Cu_3O_7$ films can be synthesized by the coevaporation of Y, Cu, and BaF_2 then annealing at high temperatures in O_2 atmosphere wet with water vapor to reduce the annealing time and substrate interaction [20].

2.3. Wet chemical methods (solution preparation)

These methods included the sol-gel preparation, coprecipitation of metal ions using precipitating agents like cyanide, oxalate, carbonate, citrate, hydroxide ions, etc., and thermal treatment [21], which resulted in a single-phase material with large surface area and high homogeneity. These methods presented good advantages such as lower temperature compared to the solid-state reactions, better homogeneity, greater flexibility in forming thin films, improved reactivity and new compositions and better control of stoichiometry, particle size, and purity. Therefore, they opened new directions for molecular architecture in the synthesis of perovskites. Solution methods were classified based on the means used for solvent removal. Two classes were identified: (i) precipitation followed by filtration, centrifugation, etc., for the separation of the solid and liquid phases and (ii) thermal treatment such as evaporation, sublimation, combustion, etc., for solvent removal. There are several factors must be taken in consideration in solution methods like solubility, solvent compatibility, cost, purity, toxicity, and choice of presumably inert anions [10].

2.3.1. Precipitation

2.3.1.1. Oxalate-based preparation

This method is built on the assimilation of oxalic acid with carbonates, hydroxides, or oxides producing metal oxalates, water, and carbon dioxide as products [22]. The solubility problem is minimized as the pH of the resulting solution is close to 7. An oxidizing atmosphere like oxygen was used during calcination to avoid the formation of carbide and carbon residues [23]. Clabaugh et al. utilized an aqueous chloride solution with oxalic acid to obtain unique and novel complex compound of $BaTiO(C_2O_4)_2\ 4H_2O$ as a precursor for the preparation of finely divided and stoichiometric $BaTiO_3$ [24].

2.3.1.2. Hydroxide-based preparation

This method is often used due to its low solubility and the possible variety of precipitation schemes. The sol-gel process can be used to produce a wide range of new materials and improve their properties. It presented some advantages over the other traditional methods like chemical homogeneity, low calcination temperature, room temperature deposition, and controlled hydrolysis for thin film formation. $BaZrO_3$ powders in its pure crystalline form can be prepared by the precipitation in aqueous solution of high basicity [25]. $LaCoO_3$ was prepared by the simultaneous oxidation and coprecipitation of a mixture containing equimolar

amounts of La(III) and Co(II) nitrates producing a gel containing hydroxide then calcination at 600 °C [26].

2.3.1.3. Acetate-based preparation

Different perovskites were prepared by mixing acetate ions alone or together with nitrate ions with the metal ions salts. $La_{1-x}Sr_xCoO_3$ with x = 0, 0.2, 0.4, 0.6 [27] was prepared using acetate precursors then calcination at 1,123 K in air for 5 h. $La_{1-x}Sr_xCo_{1-y}Fe_yO_3$ [28] was prepared using iron nitrate and strontium, cobalt, and lanthanum acetates then calcination at 1,123 K in air between 5 and 10 h.

2.3.1.4. Citrate-based preparation

Citrate precursors can be used and undergo several decomposition steps in the synthesis of perovskite [29]. These steps included the decomposition of citrate complexes and removal of CO_3^{2-} and NO_3^- ions. $LaCo_{0.4}Fe_{0.6}O_3$ can be prepared by this method, and the mechanism was investigated by thermogravimetry, XRD, and IR spectroscopy.

2.3.1.5. Cyanide-based preparation

Rare earth orthoferrites ($REFeO_3$) and cobalt compounds ($RECoO_3$) were prepared using cyanides complexes via thermal decomposition of the rare earth ferricyanide and cobalticyanide compounds [30]. $LaFe(CN)_6$ $6H_2O$, $LaCo(CN)_6$ $5H_2O$, and even ferrocyanides such as $NH_4LaFe(CN)_6$ $5H_2O$ are precipitated from the aqueous solution. This method presented some advantages like control of stoichiometry and low calcination temperature. The same method was used for the preparation of europium and other rare earth hexacyanoferrate compounds [31].

2.3.2. Thermal treatment

2.3.2.1. Freeze-drying

The freeze-drying method can be achieved through the following steps: (i) dissolution of the starting salts in the suitable solvent, water in most cases; (ii) freezing the solution very fast to keep its chemical homogeneity; (iii) freeze-drying the frozen solution to get the dehydrated salts without passing through the liquid phase; and (iv) decomposition of the dehydrated salts to give the desired perovskite powder. The rate of heat loss from the solution is the most important characteristic for the freezing step. This rate should be as high as possible to decrease the segregation of ice-salt. Also, in case of multicomponent solutions, the heat loss rate should be high to prevent the large-scale segregation of the cation components [10, 12, 21].

2.3.2.2. Plasma spray-drying

This method was applicable to various precursors, including gaseous, liquid, and solid materials. It was applied for the preparation of various ceramic, electronic, and catalytic materials. It presented many advantages in terms of economy, purity, particle size distribution,

and reactivity. This method was achieved through two steps: (i) injection of the reactants and (ii) generation and interaction of the molten droplets (with substrate or with the previously generated droplets). The thick film of $YBa_2Cu_3O_x$ covering large areas was prepared via this approach, and the optimum superconducting oxide phase was obtained by varying the preparation conditions like plasma parameters, substrate temperatures, and film postdeposition treatment [32].

2.3.2.3. Combustion

A redox reaction, which is thermally induced, occurs between the oxidant and fuel. A homogenous, highly reactive, and nanosized powder was prepared by this method. When compared with the other traditional methods, a single-phase perovskite powder can be obtained at lower calcination temperatures or shorter reaction times. One of the most popular solution combustion methods is citrate/nitrate combustion, where citric acid is the fuel and metal nitrates are used as the source of metal and oxidant. It is similar to the Pechini process "sol-gel combustion method" to a large extent, but in citrate/nitrate combustion, ethylene glycol or other polyhydroxy alcohols are not used. In addition, in citrate/nitrate combustion, the nitrates are not eliminated in the form of NO_x, but they remain in the mixture with the metal-citrate complex facilitating the auto-combustion. Iron, cobalt, and cerium-perovskite can be prepared via citrate/nitrate combustion synthesis [12, 33]. In addition, uniform nanopowder of $La_{0.6}Sr_{0.4}CoO_{3-\delta}$ was prepared by the combined citrate–EDTA method, where the precursor solution was made of metal nitrates, citric acid, and EDTA under controlled pH with ammonia [34]. $La_{0.8}Sr_{0.2}Co_{0.2}Fe_{0.8}O_{3-\delta}$ [35] and Sr- or Ce-doped $La_{1-x}M_xCrO_3$ catalysts [36] were prepared by citrate/nitrate combustion method. Furthermore, the Pechini "citrate gel" process includes two stages: (i) a complex was formed between the metal ions and citric acid, then (ii) the produced complex was polyesterified with ethylene glycol to maintain the metal salt solution in a gel in a homogenous state. This approach presented some advantages like high purity, minimized segregation, and good monitoring of the resulting perovskite composition. $LaMnO_3$ [37, 38], $LaCoO_3$ [39–41], and $LaNiO_3$ [42] were prepared by citric acid gel process producing nanophasic thin films [10].

2.3.2.4. Microwave synthesis

The microwave irradiation process (MIP), evolving from microwave sintering, was applied widely in food drying, inorganic/organic synthesis, plasma chemistry, and microwave-induced catalysis. MIP showed fascinating advantages: (i) fast reaction rate, (ii) regular heating, and (iii) efficient and clean energy. The microwave preparations were achieved in domestic microwave oven at frequency of 2.45 GHz with 1 kW as the maximum output power. Dielectric materials absorbed microwave energy converted directly into heat energy through the polarization and dielectric loss in the interior of materials [43]. The energy efficiency reached 80–90% which is much higher than the conventional routes. MIP was recently utilized to prepare perovskites nanomaterials reducing both the high temperature of calcination (higher than 700 °C) and long time (greater than 3 h) required for pretreatment or sintering [10]. $GaAlO_3$ and $LaCrO_3$ perovskites with ferroelectric, superconductive, high-temperature

ionic conductive and magnetic ordering properties, faster lattice diffusion, and grain size with smaller size were prepared in MIP [44–47]. $CaTiO_3$ powders prepared in MIP presented a fast structural ordering than powders dealt in ordinary furnace [48]. Hydrothermal conventional and dielectric heating were utilized to prepare La–Ce–Mn–O catalysts. Hydrothermal MIP leads to formation of $La_{1-x}Ce_xMnO_{3+\varepsilon}CeO_2$ ($x + \varepsilon = 0.2$) with enhanced catalytic activity [49] while using the conventional heating methods lead to formation of $LaMnO_3 + CeO_2$. Moreover, nanosized single-phase perovskite-type $LaFeO_3$ [50], $SmFeO_3$, $NdFeO_3$, $GdFeO_3$, barium iron niobate powders [51], $KNbO_3$ [52], $PbWO_4$ [53], $CaMoO_4$ [54] and MWO_4 (M: Ca, Ni) [55], strontium hexaferrite [56], and $SrRuO_3$ [57] were prepared in MIP showing finer particles, higher specific surface areas and shorter time for synthesis of single crystalline powders.

3. Doping of perovskites

The different properties of perovskites and their catalytic activity are highly affected by the method of synthesis, conditions of calcination (time, atmosphere, fuel, temperature, etc.), and A- and/or B-site substitutions. The catalytic activity of the perovskite is highly affected by partial or total substitutions on A- and/or B-site cations because of the oxidation state modification, the variation of the chemical state of the elements at A- and/or B-site, the generation of oxygen vacancies, the mobility of oxygen lattice, and the formation of structural defects [58–60]. The powerful bond between the B-site metal ions and the oxygen ions can be used to determine the basic characters of perovskites, and as a result, the B-site cation is responsible for the perovskite catalytic activity [61, 62]. Therefore, partial substitution of B-site cation with other metals M in $AB_{1-y}M_yO_3$ will display the properties of both metals: the main metal B and the dopant one M [62]. On the other hand, the cation A can stabilize the unusual oxidation states of B-site cations by the controlled formation of crystal lattice vacancies, which lead to different catalytic performances [61].

Upon doping A- and/or B-sites in ABO_3 perovskite oxides, the catalytic activity, ionic and electronic conductivity, and flexible physical and chemical properties can be altered for utilization in various applications [63–66]. Different cations with different sizes and charges can be hosted in the A- and B-sites of these perovskites; thus, many studies can be performed to utilize doped perovskites in various applications. Multiple cationic substitutions can be accepted in the stable perovskite lattice provided that Goldschmidt tolerance factor ranged between 0.75 and 1 and electroneutrality are preserved [59, 67, 68]. Therefore, variable amounts of different structural and electronic lattice defects can be accommodated in the perovskite structure as a result of their nonstoichiometry. This will further affect the activity of the perovskite and stabilize the unusual valence states of different metal ions [61, 67]. Some physical characteristics of perovskite-type oxides seriously associated with structural characters were affected greatly by the structural deformations from the ideal cubic structure of the perovskite [69].

The type of the metal ion at the B-sites and their partial substitutions can be used to determine the catalytic activity of perovskites. The substitution of B-site metal ion with various metal ions

M in the doped perovskite $AB_{1-y}M_yO_3$ showed a vast spectrum for the alteration of the catalytic and physical properties of the prepared perovskite [64, 67]. There is an effective synergism between the crystal lattice of the perovskite and the metal ions dissolved in the lattice upon doping. This synergism resulted in enhanced redox reaction and better catalytic activity of the prepared perovskite [70]. As well, a dramatic change in the transport and magnetic properties of the ABO_3 perovskite can be achieved upon doping the B-site due to an ionic valence effect and/or an ionic size effect [64]. Furthermore, upon doping the B-site in ABO_3 perovskites with transition metals especially noble metals, the stability of the perovskite was improved and the catalytic activity was enhanced greatly [71]. In addition, the incorporation of two different B ions with appropriate various charge and size may be altered the simple perovskite structure. If the two ions in B-site were used with equimolar amounts, the resulted perovskite can be represented as $AB_{0.5}B'_{0.5}O_3$ with unit cell appearing as doubled along the three axes. In addition, if B and B′ have different charges, there is a slight shift of the oxygen toward the highly charged ion in the ordered structure although the octahedral symmetry of B and B′ cations is maintained [5]. Different B-sites doped perovskites were mentioned in the literature showing enhanced catalytic properties like $LaNi_xCo_{1-x}O_3$ [72], $LaB_{0.9}Pd_{0.1}O_3$ [73], $LaMn_{1-x}PdxO_3$ [74], $BaFe_{1-x}Y_xO_{3-\delta}$ [75], $BaFe_{0.85}Cu_{0.15}O_{3-\delta}$ [76], $LaNi_{1-x}Fe_xO_3$ [77], $LaFe_{0.95-x}Co_xPd_{0.05}O_3$ [78] and $LaCo_{0.95}Pd_{0.05}O_3$ [79]. On the other hand, $(La_{1-x}Sr_x)_yMnO_{3\pm\delta}$ [80], $La_{1-x}Ce_xGaO_3$, $La_{1-x}Pr_xGaO_3$ and $La_{1-x}Nd_xGaO_3$ [81], $La_{1-x}Ca_xMnO_3$ [82], $La_{1-x}Na_xMnO_{3+\delta}$, $La1_{-x}Ca_xMnO_{3+\delta}$ [83], $(Ba_{0.93}Fe_{0.07})TiO_3$ [84], $La_{1-x}Sr_xNiO_3$, and $La_{1-x}Sr_xMnO_3$ [85] are examples of A-site doped perovskites.

4. Characterization of perovskites

X-ray powder diffraction (XRD) can be used to differentiate the different phases of the prepared perovskites. Single-crystal XRD is another analysis used to characterize the structure of the perovskite. Thermal stability of the prepared perovskites can be tested using thermal analysis techniques like TGA, DTA, and DSC. On the other hand, scanning (SEM) and transmission (TEM) electron microscopies can be utilized to identify the different morphological and surface characteristics of the prepared perovskites. Also, BET can be utilized for surface area measurement. In addition, Fourier transform infrared spectroscopy (FTIR) and X-ray photoelectron spectroscopy (XPS) can be used to completely identify the formed phases [10, 86–88].

4.1. XRD

XRD can be used for the phase identification and the relative percents of different phases of the prepared materials. Also, some structural parameters like particle size, lattice parameters (a, b, and c), lattice volume, and theoretical density can be calculated from the XRD data. Also, XRD can be used to optimize the preparation conditions of the different perovskites [3, 87–89]. Galal et al. prepared $SrPdO_3$ by citrate/nitrate combustion method at different pH values; 2, 7, and 10 at calcination temperature 750 °C for 3 h and the XRD patterns of these samples were shown in Figure 3A. The XRD data were compared with the ICCD card of $SrPdO_3$ (card number 00-025-0908). For pH 2, the experimental data and the theoretical one are well matched

http://dx.doi.org/10.5772/61280

and supported the formation of the primary orthorhombic perovskite phase of $SrPdO_3$ (the major diffraction peak 110) and the appearance of secondary phase $SrPd_3O_4$ (210). Only $SrPd_3O_4$ phase appeared in case of samples prepared at pH 7 and 10 as (110) peak disappeared. Therefore, pH 2 was the optimal pH for $SrPdO_3$ preparation. Also, the type of fuel (citric acid, urea, and glycine) used in the preparation of $SrPdO_3$ can be optimized using XRD (Figure 3B). $SrPdO_3$ was the primary phase in all cases but with different percents of $SrPdO_3$ (110) with respect to $SrPd_3O_4$ (210). The high percent was in case of urea and the small one in case of citric acid. Some structural parameters were calculated and summarized in Table 3 with good matching with theoretical data.

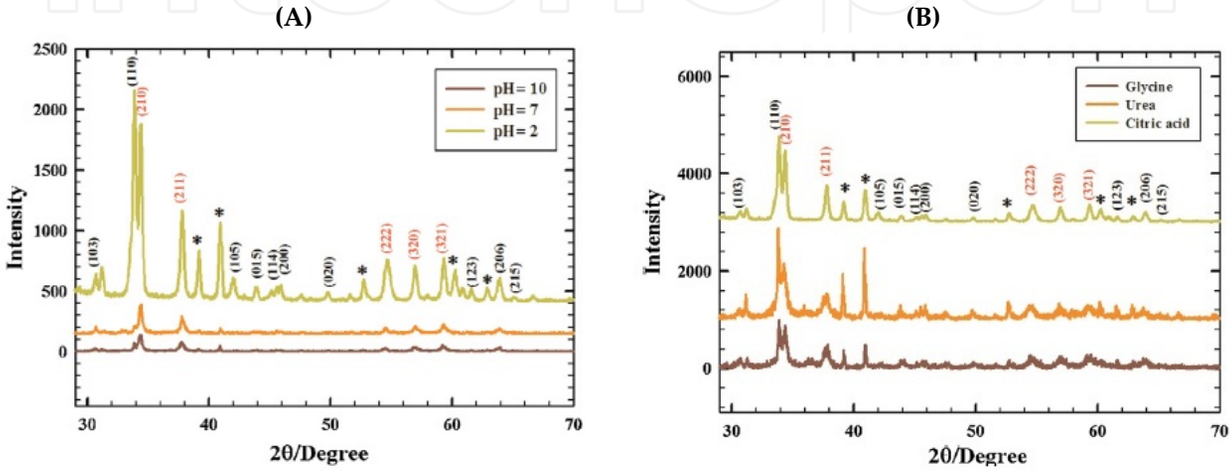

Figure 3. XRD patterns of $SrPdO_3$ prepared by combustion method at different pH values (A) and different fuels (B). Miller indices (h, l,k) are written in black line for $SrPdO_3$, red line for $SrPd_3O_4$ and the symbol (*) for $SrCl_2$. $6H_2O$ [89].

	Lattice Structure	Particle Size (nm)	Lattice Parameters (A°)	Lattice Volume (°A³)	Theoretical density (g/cm³)
Standard $SrPdO_3$ (ICCD card; 00-025-0908)	Orthorhombic		a = 3.977 b = 3.530 c = 12.82	179.98	4.47
citrate-nitrate method	Orthorhombic	34.0	a = 3.983 b = 3.541 c = 12.80	180.59	4.45
urea-nitrate method	Orthorhombic	45.4	a = 3.954 b = 3.563 c = 12.82	180.63	4.45
glycine-nitrate method	Orthorhombic	25.7	a = 3.972 b = 3.527 c = 12.83	179.69	4.47

Table 3. Structural parameters calculated from XRD data [89].

4.2. SEM and TEM

SEM and TEM can be used to study the morphology and surface characteristics of the perovskite nanomaterials. The preparation conditions, synthesis method, type of A- and B-site metal ions, and doping A- and/or B-sites affected greatly the SEM of the prepared perovskites [88–94]. Galal et al. prepared $LaNiO_3$, $LaCoO_3$, $LaFeO_3$, and $LaMnO_3$ by the microwave-assisted citrate method at 720 W as operating power for 30 min under microwave irradiation. The SEM images for the different perovskites were shown in Figure 4 presenting different morphologies depending on the kind of metal ion at B-site, respectively. $LaNiO_3$ showed compact surface with high degree of ordering while $LaCoO_3$ and $LaMnO_3$ showed spherical grains agglomerations with smaller grain size in case of $LaMnO_3$. $LaFeO_3$ showed dissimilar morphology with a porous surface containing particles with bonelike shape. In addition, $LaFeO_3$ presented greater electrocatalytic activity toward hydrogen evolution reaction compared to other types of perovskites [90].

Furthermore, the high-resolution TEM (HRTEM) can be used to show the different morphologies and particle characteristics of the different perovskites [86, 88, 95]. HRTEM images for $LaNiO_3$, $LaCoO_3$, $LaFeO_3$, and $LaMnO_3$ by the microwave-assisted citrate method were shown in Figure 5, respectively. The HRTEM images clearly showed orthorhombic phase with high crystallinity in case of $LaFeO_3$, while HRTEM images of $LaNiO_3$, $LaCoO_3$, and $LaMnO_3$ showed hexagonal distorted rhombohedral phases. The diffraction patterns obtained via HRTEM for the different perovskites were comparable with the XRD data [86, 95].

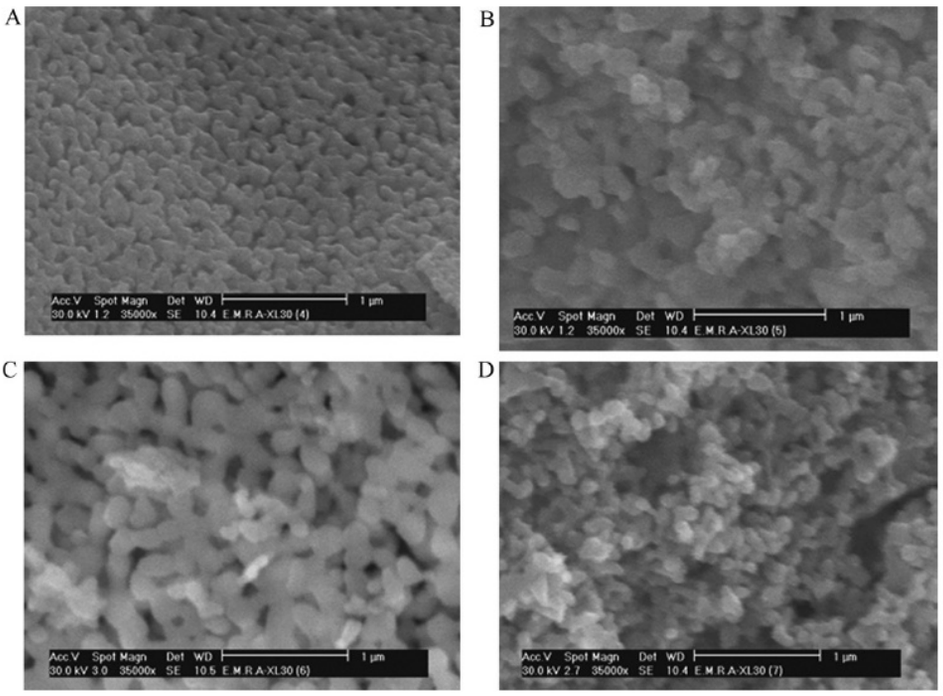

Figure 4. SEM micrographs of (A) $LaNiO_3$, (B) $LaCoO_3$, (C) $LaFeO_3$ and (D) $LaMnO_3$ prepared by the microwave-assisted citrate method at 720 W for 30 min, with a magnification of 35,000 times [90].

http://dx.doi.org/10.5772/61280

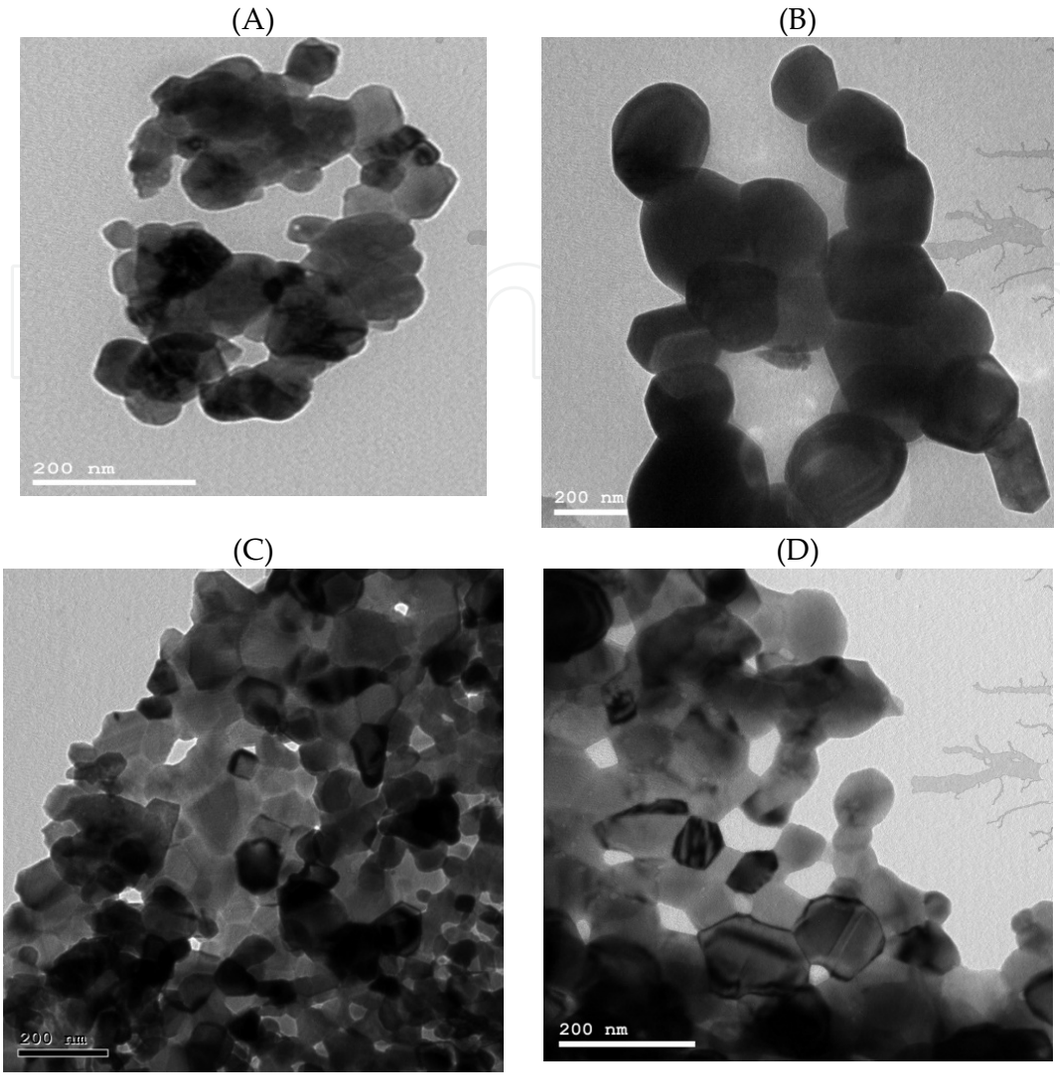

Figure 5. HRTEM micrographs of (A) $LaNiO_3$, (B) $LaCoO_3$, (C) $LaFeO_3$ and (D) $LaMnO_3$ prepared by the microwave-assisted citrate method at 720Wfor 30 min [86].

4.3. BET

The electrochemical performance and electrocatalytic activity of the perovskites are greatly associated with the specific surface area of the materials; therefore, it is necessary to measure the specific surface area of the prepared materials. The surface area values of different perovskites can be measured by Brunauer–Emmett–Teller (BET) nitrogen adsorption. The preparation conditions, synthesis method, type of A- and B-site metals, and presence of different dopants can greatly affect the surface area of the prepared perovskites [86, 87, 95]. Biniwale et al. prepared $LaFeO_3$ via different methods, namely, sol-gel, combustion, and coprecipitation and measured the corresponding surface area and the average pore diameter of the prepared perovskites. The order of decreasing the surface area of the prepared $LaFeO_3$ was sol-gel (16.5 $m^2\ g^{-1}$) > combustion (9.3 $m^2\ g^{-1}$) > coprecipitation method (5.4 $m^2\ g^{-1}$). The order of increasing the average pore diameter of the prepared $LaFeO_3$ was sol-gel (119 °A) <

coprecipitation method (140 °A) < combustion (205 °A). Sol-gel and combustion methods resulted in porous surface with internal pores contributing to higher surface area, while coprecipitation method resulted in less internal pores and lower surface area due to longer calcination time [87].

4.4. Thermal analysis

Thermal analysis can be utilized to identify the thermal stability and the decomposition temperature of the prepared perovskites. The optimum calcination temperature of any perovskite can be identified using thermal analysis [88, 96, 97]. Galal et al. prepared $SrPdO_3$ for the first time, and its optimum calcination temperature was investigated using TGA and DTG of the citrate complex of Sr and Pd (Figure 6A). The breakdown of the citrate complex occurs at ~330 °C through a smooth weight loss step. $SrPdO_3$ formation was achieved at ~750 °C through a sharp weight loss step [96].

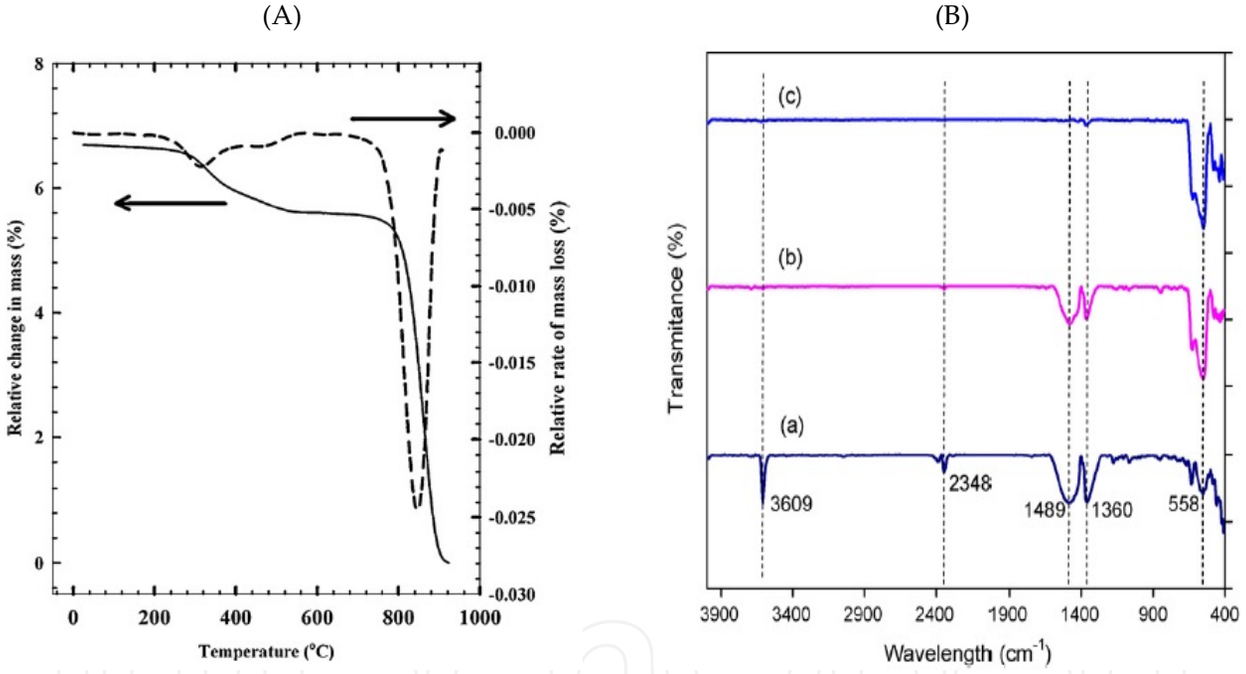

Figure 6. (A) TG spectrum of Sr and Pd mixed citrate complex, heating rate was 10 °C min^{-1} [27] and (B) FTIR spectra for $LaFeO_3$ synthesized using (a) co-precipitation method, (b) combustion method and (c) sol–gel method [87].

4.5. FTIR

The chemical bonding and chemical structure of the prepared perovskites can be investigated via FTIR. The FTIR can give structural confirmation similar to that obtained via XRD [87, 97–100]. Biniwale et al. prepared $LaFeO_3$ via different methods: sol-gel, combustion, and coprecipitation, and the FTIR for them was shown in Figure 6B [87]. The FTIR of $LaFeO_3$ showed an absorption band at 558 cm^{-1} related to the stretching vibration mode of Fe-O. Another band appeared at 430 cm^{-1} was related to the deformation vibration mode of O-Fe-O. $LaFeO_3$

prepared via coprecipitation method showed a sharp band at 3609 cm^{-1}, which is related to La-O in lanthanum oxide. In case of the other two methods, the band at 3600 cm^{-1} disappeared indicating the formation of relatively pure perovskite phase. Other bands appeared at 1360 and 1480 cm^{-1}, indicating other phases in case of coprecipitation method. As a result and as mentioned in literature, the absorption peak around 558 cm^{-1} was related to the stretching modes of metallic oxygen bond [87, 97–100].

4.6. XPS

The surface compositions of the various components of the prepared perovskites can be identified via XPS [101–106]. Lee et al. prepared $La_{0.9}FeO_3$ and $LaFeO_3$ samples and identify their structural composition via XPS analysis [102]. Figure 7 showed the XPS spectra of La (3d), Fe (2p), and O (1s) in $La_{0.9}FeO_3$ and $LaFeO_3$ samples. The binding energy of La ($3d_{5/2}$) was 833.5 eV and 833.8 eV in case of $LaFeO_3$ and $La_{0.9}FeO_3$, respectively, corresponding to the La^{3+} ions in the form of oxide. By contrast, the binding energy of Fe ($2p_{3/2}$) was 710.2 eV for both samples corresponding to Fe^{3+} ions in the form of oxide. The Fe (2p) XPS signal cannot distinguish between Fe^{3+} and Fe^{4+}. The XPS signal of O (1s) was divided into two peaks in case of $La_{0.9}FeO_3$ appearing at 529.9 and 532.1 eV. While for $LaFeO_3$, O (1s) XPS signal was divided into three peaks appearing at 529.4, 531.9, and 534.4 eV. The O (1s) binding energy values at 529.9 and 529.4 eV in both samples are attributed to lattice oxygen species. The peaks at 532.1 and 531.9 eV are ascribed to the chemisorbed oxygen species as OH^- or O^-. The chemisorbed oxygen species appeared at binding energy higher than that of lattice oxygen species by 2.1–2.5 eV. The peak appeared at 534.4 eV in case of $LaFeO_3$ was ascribed to the adsorbed water species associated with the surface lanthanum oxide which is highly hygroscopic [102].

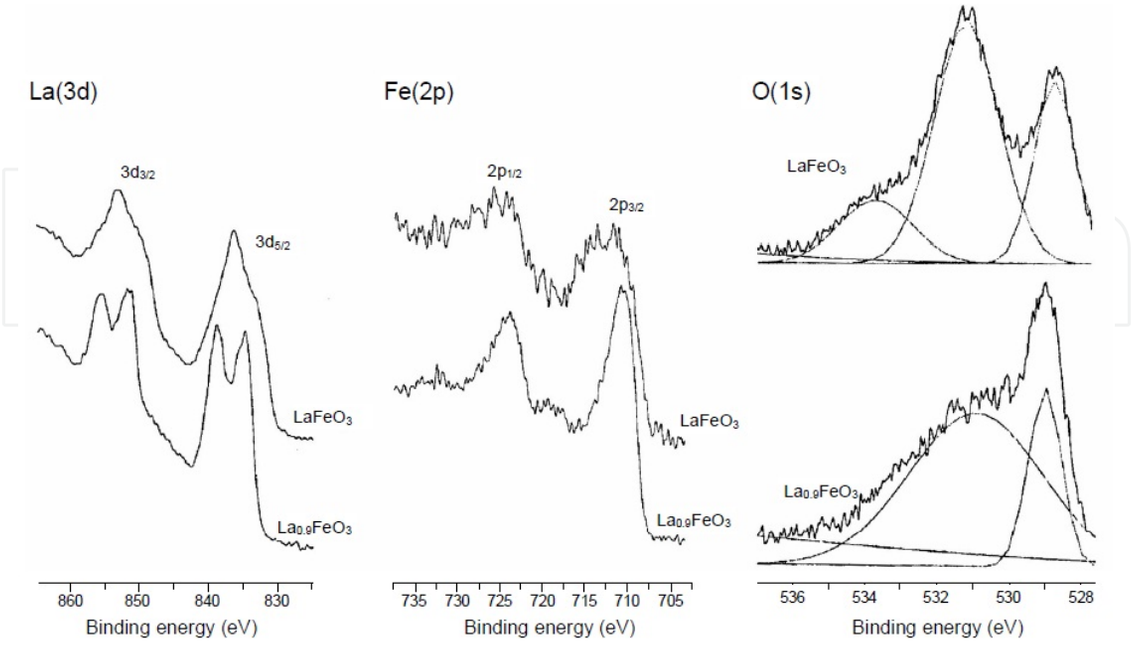

Figure 7. XPS spectra of La(3d), Fe(2p) and O(1s) in $La_{0.9}FeO_3$ and $LaFeO_3$ samples [102].

5. Applications of perovskites

Inorganic perovskite-type oxides exhibited attractive physical and chemical characteristics such as electronic conductivity, electrically active structure, the oxide ions mobility through the crystal lattice, variations on the content of the oxygen, thermal and chemical stability, and supermagnetic, photocatalytic, thermoelectric, and dielectric properties. They are fascinating nanomaterials for wide applications in catalysis, fuel cells, and electrochemical sensing. The catalytic activity of these oxides is higher than that of many transition metals compounds and even some precious metal oxides.

Nanoperovskites are recently utilized in electrochemical sensing of alcohols, gases, amino acids, acetone, glucose, H_2O_2, and neurotransmitters exhibiting good selectivity, sensitivity, unique long-term stability, excellent reproducibility, and anti-interference ability. Moreover, they have been utilized as catalysts in oxygen reduction and hydrogen evolution reactions exhibiting high electrocatalytic activity, lower activation energy, and high electron transfer kinetics. In addition, some perovskites are promising candidates for the development of effective anodic catalysts for direct fuel cells showing high catalytic performance.

5.1. Sensors and biosensors

5.1.1. Gas sensors

There are a number of requirements that the materials utilized as gas sensors must satisfy, namely, good resemblance with the target gases, manufacturability, hydrothermal stability, convenient electronic structure, resistance to poisoning, and adaptation with existing technologies. There is a wide variety of materials that can be used as gas sensors like semiconductors, namely, SnO_2, In_2O_3, and WO_3, and perovskite oxides, namely, $LaFeO_3$ and $SrTiO_3$. Perovskite oxides are fascinating materials as gas sensors due to their perfect thermal stability, ideal band gap "3–4 eV," and difference in size between the cations of A- and B-sites, allowing different dopants addition for controlling semiconducting properties and their catalytic properties. Perovskites including titanates, ferrites, and cobaltates were utilized as gas sensors for detecting CO, NO_2, methanol, ethanol, and hydrocarbons [107–110]. $LaCoO_3$ prepared via high-energy ball milling exhibited the highest amount of grain boundaries, the best CO gas sensing properties, and the smallest crystallite size of 11 nm compared to that prepared via solid-state and sol-gel reactions. The maximum response ratio increased to 26% in case of milling method with maximum response ratio temperature of 125 °C compared to 7% and 17% in case of solid-state reaction and sol-gel method. In addition, the specific surface area increased greatly from 4 $m^2 g^{-1}$ to 66 $m^2 g^{-1}$ by extra milling step, and the mobility of the oxygen was enhanced by growing the extra milling step and surface area [107]. A summary of various perovskite oxides for different gas sensing was given in Table 4.

5.1.2. Glucose sensor

It is very important to analytically determine H_2O_2 and glucose in many fields like food, clinic, and pharmaceutical analyses. H_2O_2 is considered one of the most important oxidizing agents

http://dx.doi.org/10.5772/61280

Perovskite	Sensing for	Response ratio %	Oxide type	Reference
$LaCoO_3$	CO	75% for 100 ppm CO in dry air at 125 ◦C	p-type	[107]
$La_{0.9}Ce_{0.1}CoO_3$	CO	240 % with respect to 100ppm CO in air	p-type	[108]
$NdFe_{1-x}Co_xO_3$	CO	1215% at 170 ºC for 0.03% CO gas	When x<0.3; p-type conduction behavior, when x > 0.3; n-type.	[109]
$La_{0.8}Pb_{0.2}Fe_{0.8}Cu_{0.2}O_3$	CO	Not reported	p-type	[111]
$La_{0.8}Pb_{0.2}FeO_3$	methanol	146.6 at 230 ◦C for 400 ppm methanol	p-type	[112]
$LaFeO_3$	ethanol	Not reported	p-type	[113]
$LaMg_{0.1}Fe_{0.9}O_3$	ethanol	Not reported	p-type	[114]
$SrFeO_3$	ethanol	Not reported	p-type	[115]
$SmFe_{0.9}Mg_{0.1}O_3$	ethanol	Not reported	p-type	[116]
$LaMnO_3$	ethanol	Not reported	Not reported	[117]
$La_{0.875}Ba_{0.125}FeO_3$	ethanol	sensitivity to 500 ppm ethanol is 58 at 170 °C	p-type	[118]
$Ca_xLa_{1-x}FeO_3$	ethanol	Not reported	Not reported	[119]
$LaCo_{0.1}Fe_{0.9}O_3$	ethanol	Not reported	p-type	[120]
$LaFeO_3$	ethanol	Not reported	p-type	[121]
$La_{1-x}Pb_xFeO_3$	ethanol	80% for 100 ppm in a wide temperature range of 140–240 ◦C	x = 0.30; p-type, x = 0.32–0.50; n-type	[122]
$LaFeO_3$ and $SmFeO_3$	NO_2, CO	Not reported	p-type	[123]
$LaFeO_3$	NO_2	Not reported	Not reported	[124]
$LaFeO_3$	NO_x	Not reported	Not reported	[125]
$SrTi_{1-x}Fe_xO_{3-\delta}$	hydrocarbons	Not reported	p-type	[126]
$LnFeO_3$ (Ln = La, Nd and Sm)	hydrocarbons	Not reported	p-type	[127]

Table 4. A summary of different perovskites for gas sensing.

in chemical and food industries. Glucose is a fundamental metabolite for most of the living organisms and for the clinical examination of diabetes mellitus, a worldwide health problem.

As a result, it is very important to construct biosensors for the sensitive determination of H_2O_2 and glucose [128–137]. Different types of enzymatic glucose sensors were constructed and used in the literature exhibiting the advantages of simplicity and sensitivity. However, enzymatic glucose sensors suffered from the lack of stability and the difficult procedures required for the effective immobilization of enzyme on the electrode surface. The lack of enzyme stability was attributed to its intrinsic nature because the enzyme activity was highly affected by poisonous chemicals, pH, temperature, humidity, etc. As a result, most attention was given for sensitive, simple, stable, and selective nonenzymatic glucose sensor. Different novel materials were proposed for the electrocatalytic oxidation of glucose like noble nanometals, nanoalloys, metal oxides, and inorganic perovskite oxides. Inorganic perovskite oxides as nanomaterials exhibited fascinating properties for glucose sensing like ferroelectricity, superconductivity, charge ordering, high thermopower, good biocompatibility, catalytic activity, and the ability of the perovskite structure to accommodate different metallic ions [128–137]. Zhen Zhang et al. utilized carbon paste electrode modified with $Co_{0.4}Fe_{0.6}LaO_3$ as a promising nonenzymatic H_2O_2 and glucose sensor. This sensor displayed perfect electrocatalytic activity toward H_2O_2 and glucose oxidation in alkaline medium due to the presence of large amount of active sites in the modifier. The linear dynamic range for H_2O_2 at this surface was 0.01 to 800 μM with low detection limit of 2.0 nM. For glucose, two ranges were obtained from 0.05 to 5 μM and from 5 to 500 μM with detection limit of 10 nM. The proposed sensor exhibited rapid response, excellent long-term stability, and anti-interference ability toward ascorbic acid, uric acid, and dopamine [132]. Furthermore, Atta et al. have recently modified $SrPdO_3$ perovskite with a film of gold nanoparticles to be utilized as a nonenzymatic voltammetric glucose sensor. The studied sensor exhibited high electrocatalytic activity toward glucose oxidation exploring the effective synergism between $SrPdO_3$ and gold nanoparticles. $SrPdO_3$ perovskite facilitated the charge transfer process and acted as an effective supporting substrate for gold nanoparticles. The catalytic activity of $SrPdO_3$ was attributed to the deficiency of the surface for oxygen which resulted in enhanced intrinsic reactivity toward glucose oxidation. Another reason for the catalytic activity of $SrPdO_3$ was the matrix effect induced by the stable crystal structure of the perovskite where there is a homogenous distribution of Pd^{4+} cations in the inert matrix of the perovskite during the reaction. This nanocomposite showed good performance toward glucose sensing in terms of highly reproducible response, high sensitivity, wide linearity, low detection limit, good selectivity, long-term stability, and applicability in real urine samples and blood serum [137]. A summary of different types of perovskites used for enzymatic and nonenzymatic H_2O_2 and glucose sensing was given in Table 5, exhibiting high sensitivity, wide linear range, low detection limit, anti-interference ability, applicability in real samples, and long-term stability.

5.1.3. Neurotransmitters sensor

Dopamine (DA) is an essential catecholamine neurotransmitter that exists in the mammalian central nervous system. The depletion of DA can lead to Parkinson's disease; therefore, its determination is very crucial. The interference of ascorbic acid (AA) and uric acid (UA) with DA is the major problem in DA detection [89, 140–143]. Therefore, it is very important to present a modified surface which can be sensitively and selectively detect DA even in presence

http://dx.doi.org/10.5772/61280

Perovskite	Sensing for	Sensor type	Detection limit	Sensitivity	Reference
graphite/$SrPdO_3$/Au_{nano}	glucose	Non-enzymatic	10.1 μmol L^{-1}	422.30 μA/ $mmolL^{-1}$	[137]
$LaTiO_3$-Ag0.1	glucose	Non-enzymatic	2.50×10^{-9} M	7.80×10^2 μA $mM^{-1}cm^{-2}$	[128]
$LaNi_{0.5}Ti_{0.5}O_3/CoFe_2O_4$	H_2O_2	Non-enzymatic	23 nM	3.21 μA μM^{-1} cm^{-2}	[129]
$LaNi_{0.6}Co_{0.4}O_3$	H_2O_2 and glucose	Non-enzymatic	1 nM H_2O_2 8 nM glucose	1812.84 μA mM^{-1} cm^{-2} for H_2O_2 and 643.0 μA mM^{-1} cm^{-2} for glucose	[130]
CPE–$La_{0.66}Sr_{0.33}MnO_3$–GO_x (glucose oxidase)	glucose	Enzymatic	Not reported	158.1 μAmol^{-1} L	[131]
$Co_{0.4}Fe_{0.6}LaO_3$	H_2O_2 and glucose	Non-enzymatic	2 nM H_2O_2 and 10 nM glucose	Not reported	[132]
$LaTiO_3$–Ag0.2	glucose	Non-enzymatic	2.1×10^{-7} M	784.14 μA mM^{-1} cm^{-2}	[133]
$LaNi_{0.5}Ti_{0.5}O_3$–$NiFe_2O_4$	glucose	Enzymatic	0.04 mM	Not reported	[134]
$La_{0.6}Ca_{0.4}Ni_{0.7}Fe_{0.3}O_3$	H_2O_2	Non-enzymatic	Not reported	Not reported	[135]
$La_{0.5}Sr_{0.5}CoO_{3-\delta}$	H_2O_2	Non-enzymatic	Not reported	Not reported	[136]
$La_{0.7}Sr_{0.3}NiO_3$ /chitosan/GCE	H_2O_2	Enzymatic	9.0×10^{-8} mol/L	Not reported	[138]
$LaNiO_3$	H_2O_2 and glucose	Non-enzymatic	33.9 nM H_2O_2	Not reported	[139]

Table 5. A summary of different perovskites for H_2O_2 and glucose sensing.

of high concentration of AA and UA. Atta et al. presented carbon paste electrode modified with $SrPdO_3$ (CpE/$SrPdO_3$) as a promising electrochemical DA sensor in biological fluids with unique long-term stability and low detection limit of 9.3 nmol L^{-1}. CpE/$SrPdO_3$ can simultaneously detect DA in the presence of high concentrations of AA and UA and can successfully detect DA in human urine samples with excellent recovery results in terms of selectivity, accuracy, precision, and detection limit. The proposed sensor showed high sensitivity, good selectivity, and anti-interference ability [89]. Moreover, higher response toward DA oxidation was achieved at CpE/$SrPdO_3$ compared to electrodeposited palladium nanoparticles modified CpE (CpE/Pd) with equivalent loading of Pd^{4+} salt. The higher catalytic activity at CpE/$SrPdO_3$ was explained in terms of the oxygen–surface interaction between the oxygen atoms of the hydroxyl groups and the transition element in the perovskite. One characteristic of perovskite is the deficiency of its surface for oxygen. As a result, the "dihydroxy"-oxygen adsorb onto perovskite surface with the formation of a "moderate" bond between oxygen

atoms and the transition element in the oxide [89]. Furthermore, the descriptor that controls the catalytic process in perovskites is the type of transition metal in the perovskite, which is related to the number of occupied d orbital states of a specific symmetry, for example, of the active metal. This is associated with the surface ability to bond oxygen on the basis of the calculations of the density functional theory. Therefore, the oxygen adsorption energy represented a perfect descriptor for the oxidation of DA at CpE/$SrPdO_3$. A summary of different perovskites used for neurotransmitters sensing was given in Table 6.

Perovskite	Sensing for	Linear dynamic range	Detection limit (nM)	Reference
$LaFeO_3$ microspheres made up of nanospheres	DA	$2 \times 10^{-8} – 1.6 \times 10^{-6}$ M	59	[140]
CpE/$SrPdO_3$	DA	7 – 70 μmol L^{-1}	9.3	[89]
Graphite/$SrPdO_3$	L-dopa EP, NE, DA, DOPAC and ST	0.6 – 9 μmol L^{-1}	1.63	[141]
$LaFeO_3$ nanostructure dendrites	DA	$8.2 \times 10^{-8} – 1.6 \times 10^{-7}$ M	62	[142]
$LaFeO_3$ nanoparticles	DA	$1.5 \times 10^{-7} – 8.0 \times 10^{-4}$ M	30	[143]

Table 6. A summary of different perovskites for neurotransmitters sensing.

5.2. Solid oxide fuel cells

Fuel cells have come into view as efficient alternatives to combustion engines due to their potential to minimize the environmental influence of the use of fossil fuels. A fuel cell uses certain type of chemical fuel as its energy source, and there is a direct transformation of chemical energy into electrical energy like a battery. Fuel cells are attractive because of their great efficiency, modular and distributed nature, low emissions, zero noise pollution, and role in any future hydrogen fuel economy. There are several types of fuel cells depending on operating temperature, fuel type, electrolyte type, and mobile ions. Polymer electrolyte membrane fuel cells, molten carbonate, phosphoric acid or alkali fuel cells, and solid oxide fuel cell are the most common examples of fuel cells [144]. Table 7 contained some fuel cells types and some selected features [144]. Here we will concern on solid oxide fuel cells. Solid oxide fuel cells (SOFCs), based on conducting electrolyte in the form of an oxide-ion, can generate electricity and heat and they are considered as energy-saving, environment-friendly, and effective energy conversion devices. SOFCs exhibited several features compared to the other types of fuel cells like high-energy conversion efficiency, cheap materials, low sensitivity to the fuel impurities, low pollution emissions, environmental compatibility, and excellent fuel flexibility [145–160]. Figure 8 showed the working principle of a solid oxide fuel cell [157]. The high temperature of SOFC operation resulted in the difficult choice of the proper materials

http://dx.doi.org/10.5772/61280

and the decreased cell durability. Thus, providing materials for SOFCs with good performance at intermediate temperatures (500–800 °C) is very essential so that the cell cost and the startup and shut down time can be reduced and its long-term stability can be improved [148, 155]. Perovskite oxides exhibited fascinating properties like good electrical conductivity similar to that of metals, high ionic conductivity, and perfect mixed ionic and electronic conductivity. Depending on the differences in the electrical conductive characteristics of perovskites, they are chosen as an effective component in SOFC [9]. In addition, mixed-conduction perovskite oxides possess beneficial electrochemical reaction; structural, thermal, and chemical stabilities; high electrical conductivity; high catalytic activity toward the oxygen reduction; and ideal mixed electronic and ionic conductivities to be used as effective component for intermediate temperatures SOFC (IT-SOFC) [147–160]. Shao and Haile utilized $Ba_{0.5}Sr_{0.5}Co_{0.8}Fe_{0.2}O_{3-\delta}$ as an effective cathode for intermediate SOFC with the fuel of humidified H_2 and the cathode gas of air. This cathode exhibited 1010 and 402 mW cm^{-2} as the maximum power density at 600 and 500 °C, respectively [145]. On the other hand, Goodenough reported the use of double perovskite $Sr_2MgMnMoO_{6-\delta}$ as an anode material for SOFC with dry methane as the fuel and 438 mW cm^{-2} as the maximum power density at 800 °C. This anode material showed long-term stability, stability in reducing atmosphere, tolerance to sulfur, and characteristic of oxygen deficiency [161]. Table 8 contained a summary of different perovskites used as anode and cathode for SOFC illustrating the fuel type, the operating temperature, and the maximum power density.

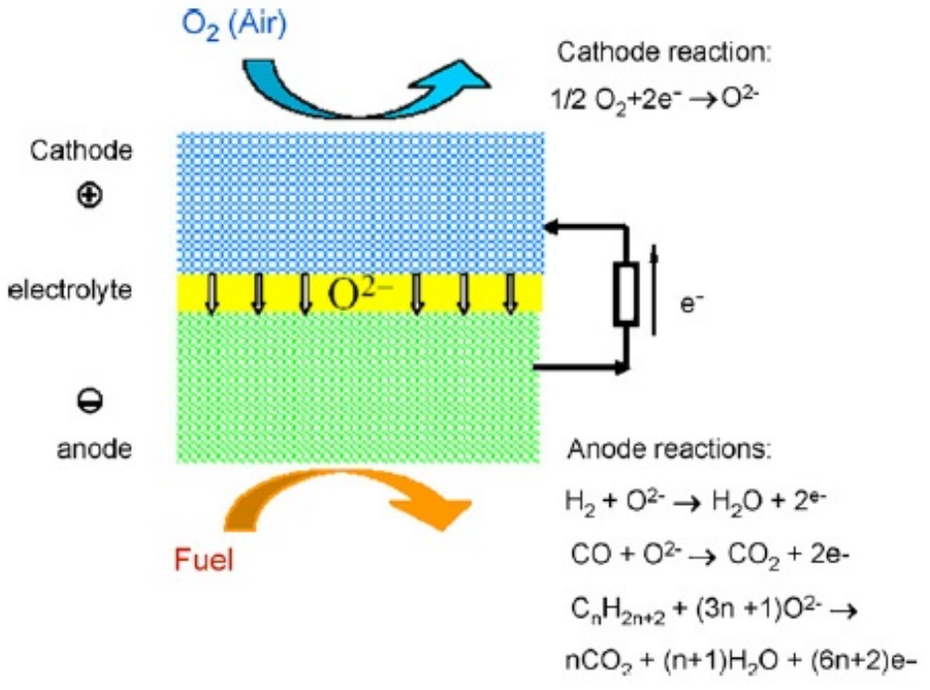

Figure 8. Schematic diagram showing the working principle of a solid oxide fuel cell [157].

Type	Temperature °C	Fuel	Electrolyte	Mobile ion
PEM: polymer electrolyte membrane or proton exchange membrane	70–110	H_2, methane	Sulphonated polymer (Nafion)	$(H_2O)_nH^+$
AFC: Alkali fuel cell	100–250	H_2	Aqueous KOH	OH^-
PAFC: Phosphoric acid fuel cell	150–250	H_2	H_3PO_4	H^+
MCFC: Molten carbonate fuel cell	500–700	Hydrocarbons, CO	$(Na, K)_2CO_3$	CO_3^{2-}
SOFC: Solid oxide fuel cell	700–1000	Hydrocarbons, CO	$(Zr, Y)O_{2-\delta}$	O^{2-}

Table 7. Fuel cell types and selected features [144].

Perovskite	Anode/cathode in the cell	Fuel used	Operating temperature °C	Maximum power density mW cm^{-2}	Reference
$Ba_{0.5}Sr_{0.5}Co_{0.8}Fe_{0.2}O_{3-\delta}$	Cathode	Humidified H_2 (~3% H_2O)	600 500	1010 402	[145]
$Ba_{0.5}Sr_{0.5}Co_{0.2}Fe_{0.8}O_{3-\delta}$	Cathode	Humidified H_2	800	266	[147]
$La_{0.7}Sr_{0.3}Co_{0.5}Fe_{0.5}O_3$	Cathode	Not reported	Not reported	Not reported	[148]
$La_{0.6}Sr_{0.4}Fe_{0.8}Co_{0.2}O_3$	Cathode	glycerol	800	Not reported	[149]
$LaBaCuFeO_{5+x}$	Cathode	Humidified H_2	700 550	327 105	[150]
$LaBaCuCoO_{5+x}$	Cathode	Humidified H_2	700 550	432 171	[150]
$Y_{0.8}Ca_{0.2}BaCoFeO_{5+\delta}$	Cathode	Humidified H_2	650	426	[151]
$NdFeO_3$	anode	sulfur vapor or SO_2	620 650	0.154 0.265	[153]
$Sm_{0.5}Sr_{0.5}CoO_{3-\delta}$	cathode	Not reported	700	936	[158]
$Sr_2Fe_{1.4}Mo_{0.6}O_{6-ı}$	cathode	H_2 or methanol	Not reported	Not reported	[159]
La0.75Sr0.25Cr0.5Mn0.5O3	anode	methane	Not reported	Not reported	[162]
$Sr_2MgMnMoO_{6-\delta}$	anode	dry methane	800	438	[161]
$La_{0.8}Sr_{0.2}Cr_{0.97}V_{0.03}O_3$	anode	dry methane	800	Not reported	[163]

Table 8. A summary of different perovskites for SOFC.

http://dx.doi.org/10.5772/61280

5.3. Catalyst

Perovskite oxides can be widely used as catalyst in modern chemical industry, exhibiting appropriate solid-state, surface, and morphological properties [6]. Several perovskites exhibited enhanced catalytic activity toward different reactions like hydrogen evolution and oxygen evolution and reduction reactions [9].

5.3.1. Hydrogen evolution reaction

Because of the advantages of high heat of combustion, abundant sources, and no pollution, hydrogen is considered as an ideal fuel. Hydrogen evolution reaction (HER) is a fascinating reaction in the renewable energy field. This reaction is very important in (i) metal electrodeposition and corrosion in acids, (ii) storage of energy through production of hydrogen, and (iii) as the hydrogen oxidation reaction reverse in low-temperature fuel cells. One of the most studied reactions in electrochemistry is the electrocatalysis in HER. The material used for HER should have (i) intrinsic electrocatalytic activity, (ii) considerable active surface area per unit volume, and (iii) good stability. To reduce the cost of electrolytic HER, the overpotential required for the operation of the electrolyzer at considerable current densities should be reduced. The overpotential reduction can be achieved through the electrode active surface area enhancement or by the selection of electrode materials of high catalytic activity. The steps of the reaction in acidic solutions are as follows:

$$M + H_3O^+ + e^- \leftrightarrow MH_{ads} + H_2O \quad (1)$$

$$MH_{ads} + H_3O^+ + e^- \leftrightarrow H_2 + M + H_2O \quad (2)$$

$$MH_{ads} + MH_{ads} \leftrightarrow H_2 + 2M \quad (3)$$

The first step in HER is the proton discharge (volume reaction, Eq. (1)), which is followed by electrodesorption step (Heyrovsky reaction, Eq. (2)) or proton recombination step, physical desorption, (Tafel reaction, Eq. (3)) [93]. Galal et al. confirmed the high catalytic activity of different perovskite oxides toward hydrogen evolution reaction [90–94, 96]. $LnFeO_3$ perovskites (Ln= Gd, La, Sm, and Nd) were prepared by the microwave assistant-citrate method, and single-phase perovskites were formed with uniform distribution of small average particle size. Tafel and electrochemical impedance measurements were used to study the catalytic activity of $LnFeO_3$ toward HER showing the effect of the type of the lanthanide ion on HER and the partial substitution effect at the La-site in $La_{1-y}Sm_yFeO_3$. The order of decreasing the catalytic activity toward HER was $NdFeO_3 > LaFeO_3 > SmFeO_3 > GdFeO_3$ based on activation energies calculations and the strength of Fe-O bond, which is related to A-type metal ion. Furthermore, the order of decreasing the catalytic activity in case of doped samples was $La_{0.75}Sm_{0.25}FeO_3 > La_{0.5}Sm_{0.5}FeO_3 > La_{0.25}Sm_{0.75}FeO_3 > LaFeO_3 > SmFeO_3$ displaying greater catalytic activity of ternary perovskites compared to that of binary ones [94]. On the other hand,

Galal et al. prepared $SrPdO_3$ by the citrate method for the first time showing enhanced catalytic activity toward HER up to 100 times with respect to the unmodified surface with 27.9 kJ mol $^{-1}$ as the calculated activation energy. The rate-determining step was the hydrogen adsorption on the catalyst and the order of the reaction at the catalyst surface was 0.86 [96]. Table 9 contained a summary of different perovskites used as catalysts for HER with the values of exchange current density at constant overpotential, activation energy, reaction order, and the rate-determining step.

Perovskite	**Exchange current density j/ μA.cm^{-2}**	**Activation energy kJ mol^{-1}**	**Reaction order**	**Rate determining step**	**Reference**
$NdFeO_3$	-107.82	24.68	0.72	adsorption of hydrogen on the catalyst	[94]
$LaFeO_3$	-367.37	41.15	0.37	adsorption of hydrogen on the catalyst	[94]
$SmFeO_3$	-147.23	57.89	0.41	adsorption of hydrogen on the catalyst	[94]
$GdFeO_3$	-451.86	81.37	0.72	adsorption of hydrogen on the catalyst	[94]
$La_{0.75}Sm_{0.25}FeO_3$	Not reported	Not reported	Not reported	adsorption of hydrogen on the catalyst	[94]
$SrPdO_3$	−946.3	27.9	0.86	adsorption of hydrogen on the catalyst	[96]
$LaFeO_3$	−105.6	51.61	0.37	adsorption of hydrogen	[90]
$LaCoO_3$	−348.9	45.37	0.74	adsorption of hydrogen	[90]
$LaNiO_3$	−158.5	41.15	0.94	adsorption of hydrogen	[90]
$LaMnO_3$	−41.9	55.05	0.87	adsorption of hydrogen	[90]
$SrRuO_3$ (microwave)	−5326.0	6.67	1.14	adsorption of hydrogen	[92]
$SrRuO_3$ (sol-combustion)	−425.5	49.45	0.98	adsorption of hydrogen	[92]
$SrRuO_3$ (coprecipitation)	−298.0	86.32	0.88	adsorption of hydrogen	[92]
$CaRuO_3$ (coprecipitation)	-1064.9	42.60	0.94	adsorption of hydrogen	[93]
$BaRuO_3$ (coprecipitation)	-3687.2	17.68	1.03	adsorption of hydrogen	[93]

Table 9. A summary of different perovskites for HER catalysis.

http://dx.doi.org/10.5772/61280

5.3.2. Oxygen reduction and oxygen evolution reactions

Oxygen reduction reaction (ORR) and oxygen evolution reaction (OER) are considered one of the most important electrode reactions in many industrial processes like fuel cells, metal electrowinning, water electrolysis, electro-organic synthesis, cathodic protection, and rechargeable metal air batteries [95, 164–166]. Platinum-based catalysts and precious metal oxides are the most common catalysts for ORR or OER, but they are expensive and scarce. Therefore, it is very important to develop other catalysts for ORR or OER. Mixed metal perovskite oxides of transition and rare earth metals are promising low-cost alternatives to precious metal catalysts for both ORR and OER [165]. Perovskite oxide exhibited unique electronic and magnetic properties, defective structure, and good cation ordering resulting in disorder-free channels of oxygen vacancies and enhanced mobility of oxygen ions [164]. Some perovskite oxides were reported as electrocatalysts for ORR and OER and summarized in Table 10 [95, 164–166]. Ruizhi Yang et al. prepared $Ba_{0.5}Sr_{0.5}Co_{0.8}Fe_{0.2}O_3$ by sol-gel method and utilized it as ORR or OER catalyst in basic medium of KOH. The proposed catalyst exhibited higher catalytic activity toward OER than the unmodified electrode [164]. Furthermore, Galal et al. prepared $LaFeO_3$ by microwave-assisted citrate method and studied its catalytic activity toward OER in acid medium of $HClO_4$. $LaFeO_3$ exhibited greater electrocatalytic activity toward OER by about 100-folds compared to the unmodified electrode. The current density at 1.5 V increased from 3.6×10^{-5} in case of unmodified electrode to 1.2×10^{-3} A/cm^2 in case of modified one. The calculated activation energy was 20 kJ/mol, which is much lower than that reported for other iron compounds and even some precious metal oxides like RuO_2. This was attributed to the matrix effect induced by the stable crystal structure of the perovskite [95]. In addition, $La_{0.6}Ca_{0.4}CoO_3$, prepared by the sol-gel method, showed high catalytic activity and relative stability toward oxygen electrochemistry in basic medium of KOH. $La_{0.6}Ca_{0.4}CoO_3$ exhibited single-phase perovskite structure, high conductivity, and large surface area [165, 166].

Perovskite	Medium	Exchange current density mA.cm^{-2}	Activation energy kJ mol^{-1}	Reaction order	Rate determining step	Reference
$LaFeO_3$	$HClO_4$	1.24×10^{-5}	20.13	0.82	Difficult to be determined	[95]
$Ba_{0.5}Sr_{0.5}Co_{0.8}Fe_{0.2}O_3$	KOH	Not reported	Not reported	Not reported	Not reported	[164]
$La_{0.6}Ca_{0.4}CoO_3$	KOH	Not reported	Not reported	Not reported	Not reported	[165]
$La_{1-x}Ca_xCoO_3$ series ($0 < x < 0.6$)	KOH	Not reported	Not reported	Not reported	Not reported	[166]

Table 10. A summary of different perovskites for ORR or OER catalysis.

5.4. Solar cells

Solar energy is a green source of energy that can be used instead of energy sources based on fossil fuels. Solar radiation can be directly converted into electrical energy in a suitable way

creating various applications for solar energy. Solar energy can be efficiently converted into electricity using photovoltaic solar cells based on silicon. The obvious disadvantage of silicon-based solar cell is the high price of electricity generated from it so that there is a potential need to develop solar cell with low cost. Recently, attention was paid to solar cells based on organic/inorganic solid-state methylammonium lead halide (CH3NH3PbX3, X=Br, I) hybrid perovskite. This type of solar cells presented effective points such as a conversion efficiency of about 20%; its cost is lower than that of conventional silicon solar cells and the availability of the raw materials. These 3D organometal halide perovskite exhibited excellent intrinsic properties for photovoltaic applications like excellent stability, appropriate band gap (~1.55 eV), high absorption coefficient (1.5×10^4 cm^{-1} at 550 nm), long hole-electron diffusion length (~100 nm for $CH_3NH_3PbI_3$ and ~1 μm for $CH_3NH_3PbI_{3-x}Cl_x$), high carrier mobility and transport, charge carriers with small effective mass, low temperature of processing, and easy processing steps [167–179]. Figure 9A showed the structure of ABX_3 perovskite (X = oxygen, carbon, nitrogen or halogen), where A and B cations are placed in a cubo-octahedral and an octahedral site, respectively. A is usually divalent and B is tetravalent when O^{2-} anion is used. On the other hand, Figure 9B showed the structure of $CH_3NH_3PbI_3$ halide perovskite where the A-site is occupied by $CH_3NH_3^+$ (organic component) and B-site cation is occupied by Pb^{2+}. As indicated by the example, halide perovskites contain monovalent and divalent cations in A- and B-sites, respectively, to maintain electrical neutrality [169, 171]. Like oxide perovskite, the tolerance factor of halide perovskite should be as close to one to maintain a stable and symmetrical crystal structure [169].

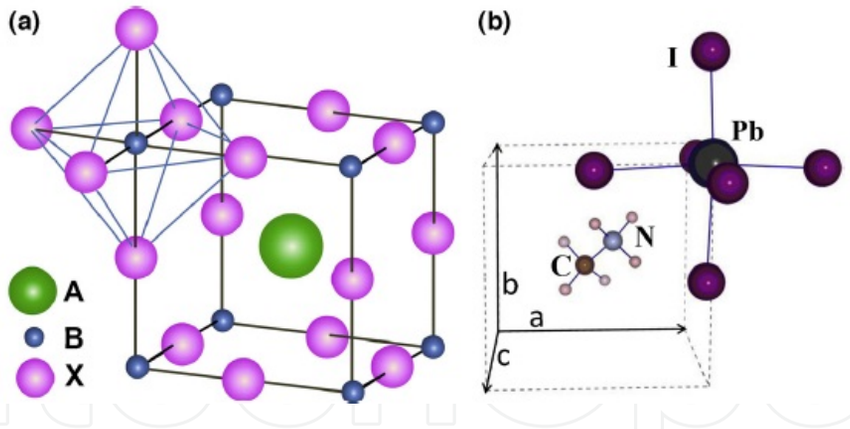

Figure 9. (a) ABX_3 perovskite structure showing BX_6 octahedral and larger A cation occupied in cubo-octahedral site. (b) Unit cell of cubic $CH_3NH_3PbI_3$ perovskite [171].

The quality of the perovskite film is very crucial for solar cells. Several methods have been used to form perovskite films with high quality such as single step solution method, vapor assistant solution process, sequential deposition of inorganic and organic precursor, and coevaporation of the precursors [167]. $CH_3NH_3PbI_3$ perovskite film was prepared with high quality by adding small amounts of N-methyl-2-pyrrolidone and a mixture of g-butyrolactone and dimethylsulfoxide via a solution method. A power conversion efficiency of 11.77% with fill factor of 80.52% was obtained based on the structure of ITO/PEDOT:PSS (poly(3,4-

ethylenedioxythiophene):polystyrenesulfonate)/perovskite/ PCBM (fullerene-derivative phenyl-C61-butyric acid methyl ester)/Ca/Al under one sun illumination (100 mW cm^{-2}) [167]. Table 11 contained a summary of different models based on perovskites used for solar cells applications with the values of power conversion efficiency, fill factor, method of perovskite formation, solar cell composition, cost, and stability.

Solar cell composition	Perovskite formation	Power conversion efficiency	Fill factor	Cost	Stability	Reference
ITO/PEDOT:PSS/ $CH_3NH_3PbI_3$ perovskite/ PCBM/Ca/Al	Solution method	11.77 %	80.52 %	low	highly stable	[167]
conducting polymer (poly-aniline) $CH_3NH_3PbI_3$ perovskite	Solution method	21 %	Not reported	low	Not reported	[168]
Mesoporous TiO_2/ $CH_3NH_3PbI_3$/ graphite paste	Solution method	1.11 %	44.5 %	low	slightly stable	[174]
Ti foil/TiO_2 nanotubes (TNTs) with organic– inorganic halide perovskite absorber "$CH_3NH_3PbI_3$" and transparent carbon nanotube electrode	Solution method	8.31 %	64 %	low	highly stable	[175]
ITO/conductive-polymer/ $CH_3NH_3PbI_3$/C_{60}/BCP/Ag	Solution method	16.5 %	75 %	low	highly stable	[177]
glass/ITO/RGO/ $CH_3NH_3PbI_3$/$PC_{61}BM$/ bathocuproine (BCP)/Ag	Solution method	10.8 %	71.6 %	low	highly stable	[179]

Table 11. A summary of different models based perovskites for Solar cells applications

6. Conclusions

Inorganic perovskite-type oxides are excellent nanomaterials for wide applications in catalysis, fuel cells, and electrochemical sensing, exhibiting attractive physical and chemical characteristics. They showed electronic conductivity, electrically active structure, the oxide ions mobility through the crystal lattice, variations on the content of the oxygen, thermal and chemical stability and supermagnetic, photocatalytic, thermoelectric, and dielectric properties. Nanoperovskites have been utilized as catalysts in oxygen reduction and hydrogen evolution

reactions exhibiting high electrocatalytic activity, lower activation energy and high electron transfer kinetics. In addition, some perovskites are promising candidates for the development of effective anodic catalysts for direct fuel cells showing high catalytic performance. Moreover, they are recently utilized in electrochemical sensing of alcohols, gases, glucose, H_2O_2, and neurotransmitters. They can enhance the catalytic performance in terms of unique long-term stability, sensitivity, excellent reproducibility, selectivity, and anti-interference ability. In addition, organometallic halide perovskites exhibited efficient intrinsic properties to be utilized as a photovoltaic solar cell with good stability and high efficiency.

Acknowledgements

The authors would like to acknowledge the financial support from Cairo University through the Vice President Office for Research Funds.

Author details

Nada F. Atta*, Ahmed Galal and Ekram H. El-Ads

*Address all correspondence to: Nada_fah1@yahoo.com

Department of Chemistry, Faculty of Science, Cairo University, Giza, Egypt

References

[1] Wolfram T, Ellialtioğlu S. Electronic and Optical Properties of d-band Perovskites. 1st ed. Cambridge University Press: New York; 2006. 1 p.

[2] Galasso FS. Structure, Properties and Preparation of Perovskite-Type Compounds. In: Smoluchowski R, Kurti N, editors. 1st ed. Pergamon Press: New York; 1969. p. 3–49. Chapter 2.

[3] Ali SMM. Synthesis of Nano-particles Using Microwave Technique, the Study of their Physical Properties and Some Applications [PhD thesis]. Faculty of Science Cairo University; 2009.

[4] Perovskite Perfect Lattice. Chapter 3. p. 79–114.

[5] Johnsson M, Lemmens P. Crystallography and Chemistry of Perovskites. 2005. p. 1–11.

[6] Peňa MA, Fierro JLG. Chemical structures and performance of perovskite oxides. Chemical Reviews. 2001;101:1981–2017. DOI: 10.1016/j.apsusc.2014.10.168.

[7] Fu1 D, Itoh M. Ferroelectrics—Material Aspects. In: Lallart M, editor. InTech: Shizuoka University, Tokyo Institute of Technology, Japan; 2011. p. 413–442. Chapter 20.

[8] Porta P, De Rossi S, Faticanti M, Minelli G, Pettiti I, Lisi L, Turco M. Perovskite-type oxides: I. Structural, magnetic, and morphological properties of $LaMn_{1-x}Cu_xO_3$ and $LaCo_{1-x}Cu_xO_3$ solid solutions with large surface area. Journal of Solid State Chemistry. 1999;146:291–304. DOI: 10.1006/jssc.1999.8326.

[9] Ishihara T. Perovskite Oxide for Solid Oxide Fuel Cells, Fuel Cells and Hydrogen Energy. In: Ishihara T, editor. Springer Science Business Media, LLC; 2009. p. 1–16. Chapter 1.

[10] Lozano-Gorrín AD. Polycrystalline Materials—Theoretical and Practical Aspects. In: Zakhariev Z, editor. Universidad de La Laguna. Spain: InTech; 2012. p 107–124. Chapter 5.

[11] Nieto S, Polanco R, Roque-Malherbe R. Absorption kinetics of hydrogen in nanocrystals of $BaCe_{2.95}Yb_{0.05}O_3$-proton conducting perovskite. Journal of Physical Chemistry C. 2007;111:2809–2818. DOI: 10.1021/jp067389i.

[12] Ecija A, Vidal K, Larrañaga A, Ortega-San-Martín L, Arriortua MI. Advances in Crystallization Processes. In: Mastai Y, editor. InTech; 2012. p. 486–506. Chapter 19.

[13] Wu J. [PhD thesis]. California Institute of Technology, Pasadena, CA; 2005.

[14] Martinez E, Viches ES, Beltran-Porter A, Beltran-Porter D. Low temperature synthesis of Ba-Fe mixed oxides having perovskite structures. Materials Research Bulletin. 1985;21:511–514. DOI: 10.1016/0025-5408(86)90103-0

[15] Dijkkamp D, Venkatesan T, Wu XD, Shaheen SA, Jisrawi N, Min-Lee YH, McLean WL, Croft M. Preparation of Y-Ba-Cu-O oxide superconductor thin films using pulsed laser evaporation from high Tc bulk material. Applied Physics Letters. 1987;51(8):619–621. DOI: 10.1063/1.98366.

[16] Webb C, Weng SL, Eckstein JN, Missert N, Char K, Schlom DG, Hellman ES, Beasley MR, Kapitulink A, Harris JS. Applied Physics Letters 1988;51:12.

[17] Croteau A, Matsubara S, Miyasaka Y, Shohata N, Ferroelectric lead zirconate titanate (Pb(Zr, Ti)O_3) thin films prepared by metal target sputtering. Japanese Journal of Applied Physics, Part 1. 1990;26:18. DOI: 10.7567/JJAPS.26S2.18.

[18] Han Z, Bourget L, Li H, Ulla M, Millman WS, Baun HP, Xu MF, Sarma BK, Levy M, Tonner BP. Single target deposition, post proceeding and electron spectroscopy of perovskite superconductor thin films. AIP Conference Proceedings. 1988;165:66. DOI: 10.1063/1.37082.

[19] Naito M, Hammond RH, Oh B, Hahn MR, Hsu JWP, Rosenthal P, Marshall AF, Beasley MR, Geballe TH, Kapitulnik A. Thin film synthesis of the high Tc oxide supercon-

ductor yttrium barium copper oxide ($YBa_2Cu_3O_7$) by electron-beam codeposition. Journal of Materials Research. 1987;2:713–725. DOI: 10.1557/JMR.1987.0713.

[20] Mankiewich PM, Scofield JH, Skocpol WJ, Howard RE, Dayem AH. Good E., Reproducible technique for fabrication of thin films of high transition temperature superconductors. Applied Physics Letters. 1987;51(21):1753–1755.

[21] Tejuca LG, Fiero JLG. Properties and Applications of Perovskite Type-Oxides. Marcel Dekker Inc. Ed. Chemical Industries. 1993;50.

[22] Gallagher PK, Fleming DA. Influence of oxygen partial pressure on the synthesis of barium yttrium copper oxide ($Ba_2YCu_3O_7$) from a novel oxalate precursor. Chemistry of Materials. 1989;1:659–664. DOI: 10.1021/cm00006a019.

[23] Gallagher PK, Schrey F. The thermal decomposition of freeze-dried tantalum and mixed lithium–niobium oxalate. Thermochimica Acta. 1970;1:465–476. DOI: 10.1016/0040-6031(70)85017-1.

[24] Clabaugh WS, Swiggard EM, Gilchrist RJ. Preparation of barium titanyl oxalate tetrahydrate for conversion to barium titanate of highly purity. Journal of Research of the National Bureau of Standards. 1956;56:289–291.

[25] Boschini F, Rulmont A, Cloots R, Vertruyen B. Rapid synthesis of submicron crystalline barium zirconate $BaZrO_3$ by precipitation in aqueous basic solution below 100 °C. Journal of the European Ceramic Society 2009;29(8):1457–1462. DOI: 10.1016/j.jeurceramsoc.2008.09.001.

[26] Barnard KR, Foger K, Turney TW, Williams RD. Lanthanum cobalt oxide oxidation catalysts derived from mixed hydroxide precursors. Journal of Catalysis. 1990;125(2): 265–275. DOI: 10.1016/0021-9517(90)90302-Z.

[27] Nakamura T, Misono M, Yoneda Y. Reduction and oxidation and catalytic properties of perovskite type mixed oxide catalysts. Chemistry Letters. 1981;1589.

[28] Zhang HM, Shimizu Y, Teraoka Y, Miura N, Yamazoe N. Oxygen sorption and catalytic properties of $La_{1-x}Sr_xCo_{1-y}Fe_yO_3$ Perovskite-type oxides. Journal of Catalysis. 1990;121(2):432–440. DOI: 10.1016/0021-9517(90)90251-E.

[29] Zhang HM, Teraoka Y, Yamazoe N. Preparation of perovskite type oxides with large surface area by citrate process. Chemistry Letters. 1987:665–668.

[30] Gallagher PK. A simple method for the preparation of $(RE)FeO_3$ and $(RE)CoO_3$. Materials Research Bulletin. 1967; 3,225–232. DOI: 10.1016/0025-5408(68)90123-2.

[31] Gallagher PK, Prescott B. Further studies of the thermal decomposition of europium hexacyanoferrate(III) and ammonium europium hexacyanoferrate(II). Inorganic Chemistry. 1970;9:2510–2512. DOI: 10.1021/ic50093a026.

[32] Cuomo JJ, Guarnieri C, Richard M, Shivashankar SA, Roy RA, Yee DS, Rosenberg R. Large area plasma spray deposited superconducting $YBa_2Cu_3O_7$ thick films. Advanced Ceramic Materials. 1989;2(3B):422–429.

[33] Deganello F, Marcì G, Deganello G. Citrate–nitrate auto-combustion synthesis of perovskite-type nanopowders: a systematic approach. Journal of the European Ceramic Society. 2009;29(3):439–450. DOI: 10.1016/j.jeurceramsoc.2008.06.012.

[34] Tao Y, Shao J, Wang J, Wang WG. Synthesis and properties of La0.6Sr0.4CoO3–δ nanopowder. Journal of Power Sources. 2008;185(2):609–614. DOI: 10.1016/j.jpowsour.2008.09.021.

[35] Park JH, Kim JP, Kwon HT, Kim J. Oxygen permeability, electrical property and stability of $La_{0.8}Sr_{0.2}Co_{0.2}Fe_{0.8}O_{3-\delta}$ membrane. Desalination. 2008;233(1–3):73–81. DOI: 10.1016/j.desal.2007.09.045.

[36] Rida K, Benabbas A, Bouremmad F, Peña MA, Sastre E, Martínez-Arias A. Effect of strontium and cerium doping on the structural characteristics and catalytic activity for C_3H_6 combustion of perovskite $LaCrO_3$ prepared by sol-gel. Applied Catalysis B: Environmental. 2008;84(3–4):457–467.

[37] Hammami R, Aïssa SB, Batis H. Effects of thermal treatment on physico-chemical and catalytic properties of lanthanum manganite $LaMnO_{3+y}$. Applied Catalysis A: General. 2009;353(2):145–153. DOI: 10.1016/j.apcata.2008.10.048.

[38] Li Y, Xue L, Fan L, Yan Y. Journal of Alloys and Compounds. (2008).

[39] Popa M, Calderón-Moreno JM. Lanthanum cobaltite thin films on stainless steel. Thin Solid Films. 2009;517(5):1530–1533. DOI: 10.1016/j.tsf.2008.08.187.

[40] Ivanova S, Senyshyn A, Zhecheva E, Tenchev K, Nickolov V, Stoyanova R, Fuess H. Mechanochemical synthesis and characterization of nanodimensional iron–cobalt spinel oxides. Journal of Alloys and Compounds. 2009;485(1):356–361. DOI: 10.1016/j.jallcom.2009.05.107.

[41] Wang J, Manivannan A, Wu N. Sol-gel derived $La_{0.6}Sr_{0.4}CoO_3$ nanoparticles, nanotubes, nanowires and thin films. Thin Solid Films 2008;517(2):582–587. DOI: 10.1016/j.tsf.2008.06.095.

[42] Rivas ME, Fierro JLG, Guil-López R, Peña MA, La Parola V, Goldwasser MR. Preparation and characterization of nickel-based mixed-oxides and their performance for catalytic methane decomposition. Catalysis Today. 2008;133–135:367–373. DOI: 10.1016/j.cattod.2007.12.045.

[43] Jin Q. Microwave Chemistry. China Science Press: Beijing; 1999.

[44] Selvam MP, Rao K. microwave synthesis and consolidation of gadolinium aluminum perovskite: a ceramic extraordinaire. Advanced Materials. 2000;12:1621–1624. DOI: 10.1002/1521-4095(200011)12:21<1621::AID-ADMA1621>3.0.CO;2-X.

[45] Gibbons KE, Blundell SJ, Mihut AI, Gameson I, Edwards PP, Miyazaki Y, Hyatt NC, Jones MO, Porch A. Rapid synthesis of colossal magnetoresistance manganites by microwave dielectric heating. Chemical Communications. 2000;1:159–160. DOI: 10.1039/A907677H.

[46] Selvam MP, Rao KJ. Microwave preparation and sintering of industrially important perovskite oxides: $LaMO_3$ (M = Cr, Co, Ni). Journal of Materials and Chemistry. 2003;13:596–601. DOI: 10.1039/B211602B.

[47] Yan H, Huang X, Lu Z, Hu H, Xue R, Chen L. Microwave synthesis of $LiCoO_2$ cathode materials. Journal of Power Sources. 1997;68:530–532. DOI: 10.1016/S0378-7753(96)02565-7.

[48] Cavalcante LS, Marques VS, Sczancoski JC, Escote MT, Joya MR, Varela JA, Santos MRMC, Pizani PS, Longo E. Synthesis, structural refinement and optical behavior of $CaTiO_3$ powders: a comparative study of processing in different furnaces. Chemical Engineering Journal. 2008;143(1–3):299–301.

[49] Kaddouri A, Gelin P, Dupont N. Methane catalytic combustion over La–Ce–Mn–O–perovskite prepared using dielectric heating. Catalysis Communications. 2009;10(7):1085–1089. DOI: 10.1016/j.catcom.2008.12.063.

[50] Farhadi S, Momeni Z, Taherimehr M. Rapid synthesis of perovskite-type $LaFeO_3$ nanoparticles by microwave-assisted decomposition of bimetallic $La[Fe(CN)_6]$ $5H_2O$ compound. Journal of Alloys and Compounds. 2009;471(1–2):L5–L8. DOI: 10.1016/j.jallcom.2008.03.113.

[51] Charoenthai N, Traiphol R, Rujijanagul G. Microwave synthesis of barium iron niobate and dielectric properties. Materials Letters. 2008;62(29):4446–4448. DOI: 10.1016/j.matlet.2008.07.047.

[52] Paula AJ, Parra R, Zaghete MA, Varela JA. Synthesis of $KNbO_3$ nanostructures by a microwave assisted hydrothermal method. Materials Letters. 2008;62(17–18):2581–2584. DOI: 10.1016/j.matlet.2007.12.059.

[53] Ryu JH, Koo S, Chang DS, Yoon J, Lim CS, Shim KB. Microwave-assisted synthesis of $PbWO_4$ nano-powders via a citrate complex precursor and its photoluminescence. Ceramics International. 2006;32(6):647–652. DOI: 10.1016/j.ceramint.2005.04.025.

[54] Ryu JH, Koo S, Chang DS, Yoon J, Lim CS, Shim KB. Microwave-assisted synthesis of $CaMoO_4$ nano-powders by a citrate complex method and its photoluminescence property Journal of Alloys and Compounds. 2005;390(1–2);245–249. DOI: 10.1016/j.jallcom.2004.07.064.

[55] Ryu JH, Yoon J, Lim CS, Oh W, Shim KB. Microwave-assisted synthesis of nanocrystalline MWO_4 (M: Ca, Ni) via water-based citrate complex precursor. Ceramics International. 2005;31(6):883–888. DOI: 10.1016/j.ceramint.2004.09.015.

[56] Fu Y, Lin C. Fe/Sr ratio effect on magnetic properties of strontium ferrite powders synthesized by microwave-induced combustion process. Journal of Alloys and Compounds 2005;386(1–2):222–227. DOI: 10.1016/j.jallcom.2004.04.148.

[57] Galal A, Darwish SA, Atta NF, Ali SM, Abd El Fatah AA. Synthesis, structure and catalytic activity of nano-structured Sr–Ru–O type perovskite for hydrogen production. Applied Catalysis A: General. 2010;378:151–159. DOI: 10.1016/j.jallcom.2004.04.148.

[58] Li Z, Meng M, Li Q, Xie Y, Hu T, Zhang J. Fe-substituted nanometric $La_{0.9}K_{0.1}Co_{1-x}Fe_xO_{3-\delta}$ perovskite catalysts used for soot combustion, NO_x storage and simultaneous catalytic removal of soot and NOx. Chemical Engineering Journal. 2010;164:98–105. DOI: 10.1016/j.cej.2010.08.036.

[59] Silva GRO, Santos JC, Martinelli DMH, Pedrosa AMG, Souza MJBd, Melo DMA. Synthesis and characterization of $LaNi_xCo_{1-x}O_3$ perovskites via complex precursor methods. Materials Sciences and Applications. 2010;1:39–45. DOI: 10.4236/msa.2010.12008.

[60] Jahangiri A, Aghabozorg H, Pahlavanzadeh H. Effects of Fe substitutions by Ni in La–Ni–O perovskite-type oxides in reforming of methane with CO_2 and O_2. International Journal of Hydrogen Energy. 2013;38:10407–10416. DOI: 10.1016/j.ijhydene.2013.05.080.

[61] Russo N, Palmisano P, Fino D. Pd substitution effects on perovskite catalyst activity for methane emission control. Chemical Engineering Journal. 2009;154:137–145. DOI: 10.1016/j.cej.2009.05.015.

[62] Oishi M, Yashiro K, Sato K, Mizusaki J, Kawad T. Oxygen nonstoichiometry and defect structure analysis of B-site mixed perovskite-type oxide (La, Sr)(Cr, M)$O_{3-\delta}$ (M=Ti, Mn and Fe). Journal of Solid State Chemistry.2008;181:3177–3184. DOI: 10.1016/j.jssc.2008.08.015.

[63] Liu X, Zhao H, Yang J, Li Y, Chen T, Lu X, Ding W, Li F. Lattice characteristics, structure stability and oxygen permeability of $BaFe_{1-x}Y_xO_{3-\delta}$ ceramic membranes. Journal of Membrane Science. 2011;383:235–240. DOI: 10.1016/j.memsci.2011.08.059.

[64] Dho J, Hur NH. Magnetic and transport properties of lanthanum perovskites with B-site half doping. Solid State Communications. 2006;138:152–156. DOI: 10.1016/j.ssc.2006.02.008.

[65] Suntivich J, May KJ, Gasteiger HA, Goodenough JB, Shao-Horn Y. A Perovskite Oxide Optimized for Oxygen Evolution Catalysis from Molecular Orbital Principles. Science. 2011;334:1383–1385.

[66] Vojvodic A, Nørskov JK. Optimizing Perovskites for the Water-Splitting Reaction. Science. 2011;334:1355–1356. DOI: 10.1126/science.1215081.

[67] Alifanti M, Auer R, Kirchnerova J, Thyrion F, Grange P, Delmon B. Activity in methane combustion and sensitivity to sulfur poisoning of $La_{1-x}Ce_xMn_{1-y}Co_yO_3$ perovskite oxides. Applied Catalysis, B. 2003;41:71–81. DOI: 10.1016/S0926-3373(02)00194-7.

[68] Kida T, Yamasaki A, Watanabe K, Yamazoe N, Shimanoe K. Oxygen-permeable membranes based on partially B-site substituted $BaFe_{1-y}M_yO_{3-\delta}$ (M=Cu or Ni). Journal of Solid State Chemistry. 2010;183:2426–2431. DOI: 10.1016/j.jssc.2010.08.002.

[69] Sora IN, Caronna T, Fontana F, Fernàndez CdJ, Caneschi A, Green M. Crystal structures and magnetic properties of strontium and copper doped lanthanum ferrites. Journal of Solid State Chemistry. 2012;191:33–39. DOI: 10.1016/j.jssc.2012.02.020.

[70] Rodríguez GCM, Saruhan B. Effect of Fe/Co-ratio on the phase composition of Pd-integrated perovskites and its H_2-SCR of NO_x performance. Applied Catalysis, B. 2010;93:304–313. DOI: 10.1016/j.apcatb.2009.10.004.

[71] Ke-bin Z, Hong-de C, Qun T, Bao-wei Z, Di-xin S, Xiao-bai X. Synergistic effect of palladium and oxygen vacancies in the Pd/perovskite catalysts synthesized by the SPC method. Journal of Environmental Sciences. 2005;17(1):19–24. PMID: 15900751.

[72] Silva GRO, Santos JC, Martinelli DMH, Pedrosa AMG, de Souza MJB, Melo DMA. Synthesis and characterization of $LaNi_xCo_{1-x}O_3$ perovskites via complex precursor methods. Materials Sciences and Applications, 2010;1:39–45. DOI: 10.4236/msa.2010.12008.

[73] Russo N, Palmisano P, Fino D. Pd substitution effects on perovskite catalyst activity for methane emission control. Chemical Engineering Journal. 2009;154:137–141. DOI: 10.1016/j.cej.2009.05.015.

[74] Li C, Jiang B, Fanchiang W, Lin Y. The effect of Pd content in $LaMnO_3$ for methanol partial oxidation. Catalysis Communications. 2011;16:165–169. DOI: 10.1016/j.catcom.2011.09.028.

[75] Liu X, Zhao H, Yang J, Li Y, Chen T, Lu X, Ding W, Li F. Lattice characteristics, structure stability and oxygen permeability of $BaFe_{1-x}Y_xO_{3-\delta}$ ceramic membranes. Journal of Membrane Science. 2011;383:235– 240. DOI: 10.1016/j.memsci.2011.08.059.

[76] Kida T, Yamasaki A, Watanabe K, Yamazoe N, Shimanoe K. Oxygen-permeable membranes based on partially B-site substituted $BaFe_{1-y}M_yO_{3-\delta}$ (M= Cu or Ni). Journal of Solid State Chemistry. 2010;183:2426–2431. DOI: 10.1016/j.jssc.2010.08.002.

[77] Jahangiri A, Aghabozorg H, Pahlavanzadeh H. Effects of Fe substitutions by Ni in LaNiO perovskite-type oxides in reforming of methane with CO_2 and O_2. International of Hydrogen Energy. 2013;38:10407–10416. DOI: 10.1016/j.ijhydene.2013.05.080.

[78] Rodrìguez GCM, Saruhan B. Effect of Fe/Co-ratio on the phase composition of Pd-integrated perovskites and its H_2-SCR of NO_x performance. Applied Catalysis B: Environmental. 2010;93:304–313. DOI: 10.1016/j.apcatb.2009.10.004.

[79] Ke-bin Z, Hong-de C, Qun T, Bao-wei Z, Di-xin S, Xiao-bai X. Synergistic effect of palladium and oxygen vacancies in the Pd/perovskites catalysts synthesized by SPC method. Journal of environmental sciences. 2005;17(1):19–24. PMID: 15900751.

[80] Poulsen FW. Defect chemistry modelling of oxygen-stoichiometry, vacancy concentrations, and conductivity of $(La_{1-x}Sr_x)MnO_{3\pm\delta}$. Solid State Ionics. 2000;129:145–162. DOI: 10.1016/S0167-2738(99)00322-7.

[81] Parveen A, Gaur NK. Effect of A-site doping on thermal properties of $LaGaO_3$. Solid State Sciences. 2012;14:814–819. DOI: 10.1016/j.solidstatesciences.2012.03.032.

[82] Srivastava A, Gaur NK, Kaur N, Singh RK. Effect of cation doping on low-temperature specific heat of $LaMnO_3$ manganite. Journal of Magnetism and Magnetic Materials. 2008;320:2596–2601. DOI: 10.1016/j.jmmm.2008.05.042.

[83] Malavasi L, Ritter C, Mozzati MC, Tealdi C, Islam MS, Azzoni CB, Flor G. Effects of cation vacancy distribution in doped $LaMnO_{3+\delta}$ perovskites. Journal of Solid State Chemistry. 2005;178:2042–2049. DOI: 10.1016/j.jssc.2005.04.019.

[84] Lin F, Shi W. Effects of doping site and pre-sintering time on microstructure and magnetic properties of Fe-doped $BaTiO_3$ ceramics. Physica B. 2012;407:451–456. DOI: 10.1016/j.physb.2011.11.013.

[85] Wei HJ, Cao Y, Ji WJ, Au CT. Lattice oxygen of $La_{1-x}Sr_xMO_3$ (M = Mn, Ni) and $LaMnO_{3-\alpha}F_\beta$ perovskite oxides for the partial oxidation of methane to synthesis gas. Catalysis Communications. 2008;9:2509–2514. DOI: 10.1016/j.catcom.2008.06.019.

[86] Abd Al-Rahman YM. Characterization and some applications of nano-inorganic oxides synthesized by microwave technique [MSc thesis]. Faculty of Science Cairo University; 2013.

[87] Gosavi PV, Biniwale RB. Pure phase $LaFeO_3$ perovskite with improved surface area synthesized using different routes and its characterization. Materials Chemistry and Physics. 2010;119:324–329. DOI: 10.1016/j.matchemphys.2009.09.005.

[88] Vijayakumar C, Kumar HP, Solomon S, Thomas JK, Warriar PRS, Koshy J. Synthesis, characterization, sintering and dielectric properties of nanostructured perovskite-type oxide, Ba_2GdSbO_6. Bulletin Materials Science. 2008;31(5):719–722. DOI: 10.1007/s12034-008-0113-2.

[89] Atta NF, Ali SM, El-Ads EH, Galal A. Nano-perovskite carbon paste composite electrode for the simultaneous determination of dopamine, ascorbic acid and uric acid. Electrochimica Acta. 2014;128:16–24. DOI: 10.1016/j.electacta.2013.09.101.

[90] Galal A, Atta NF, Ali SM. Investigation of the catalytic activity of $LaBO_3$ (B = Ni, Co, Fe or Mn) prepared by the microwave-assisted method for hydrogen evolution in acidic medium. Electrochimica Acta. 2011;56:5722–5730. DOI: 10.1016/j.electacta.2011.04.045.

[91] Galal A, Atta NF, Ali SM. Optimization of the synthesis conditions for $LaNiO_3$ catalyst by microwave assisted citrate method for hydrogen production. Applied Catalysis A: General. 2011;409–410:202–208. DOI: 10.1016/j.apcata.2011.10.005.

[92] Galal A, Darwish SA, Atta NF, Ali SM, Abd El Fatah AA. Synthesis, structure and catalytic activity of nano-structured Sr–Ru–O type perovskite for hydrogen production. Applied Catalysis A: General. 2010;378:151–159. DOI: 10.1016/j.apcata.2010.02.015.

[93] Atta NF, Galal A, Ali SM. The catalytic activity of ruthenates $ARuO_3$ (A= Ca, Sr or Ba) for the hydrogen evolution reaction in acidic medium. International Journal of Electrochemical Science. 2012;7:725–746. DOI: 71772857.

[94] Atta NF, Galal A, Ali SM. The effect of the lanthanide ion-type in $LnFeO_3$ on the catalytic activity for the hydrogen evolution in acidic medium. International Journal of Electrochemical Science. 2014;9:2132–2148. DOI: 94967196.

[95] Ali SM, Abd Al-Rahman YM, Galal A. Catalytic activity toward oxygen evolution of $LaFeO_3$ prepared by the microwave assisted citrate method. Journal of Electrochemical Society. 2012;159(9):F600–F605. DOI: 10.1149/2.063209jes.

[96] Galal A, Atta NF, Darwish SA, Abd El Fatah AA, Ali SM. Electrocatalytic evolution of hydrogen on a novel $SrPdO_3$ perovskite electrode. Journal of Power Sources. 2010;195:3806–3809. DOI: 10.1016/j.jpowsour.2009.12.091.

[97] Ghosh S, Dasgupta S. Synthesis, characterization and properties of nanocrystalline perovskite cathode materials. Materials Science—Poland. 2010;28(2):427–438.

[98] Viruthagiri G, Praveen P, Mugundan S, Gopinathan E. Synthesis and characterization of pure and nickel doped $SrTiO_3$ nanoparticles via solid state reaction route. Indian Journal of Advances in Chemical Science. 2013;1(3):132–138.

[99] Li S. Preparation and characterization of perovskite structure lanthanum gallate and lanthanum aluminate based oxides [PhD thesis]. Royal Institute of Technology Stockholm, Sweden; 2009.

[100] Pecchi G, Campos CM, Jiliberto MG, Delgado EJ, Fierro JLG. Effect of additive Ag on the physicochemical and catalytic properties of $LaMn_{0.9}Co_{0.1}O_{3.5}$ perovskite. Applied Catalysis A: General. 2009;371:78–84. DOI: 10.1016/j.apcata.2009.09.031.

[101] Lakshminarayanan N, Choi H, Kuhn1 JN, Ozkan US. Effect of additional B-site transition metal doping on oxygen transport and activation characteristics in $La_{0.6}Sr_{0.4}(Co_{0.18}Fe_{0.72}X_{0.1})O_{3-\delta}$ (where X= Zn, Ni or Cu) perovskite oxides. Applied Catalysis B: Environmental. 2011;103:318–325. DOI: 10.1016/j.apcatb.2011.01.038.

[102] Cho Y, Choi K, Kim Y, Jung J, Lee S. Characterization and catalytic properties of surface La-rich $LaFeO_3$ perovskite. Bulletin of the Korean Chemical Society. 2009;30(6):1368–1372.

[103] Pawlak DA, Ito M, Oku M, Shimamura K, Fukuda T. Interpretation of XPS O (1s) in mixed oxides proved on mixed perovskite crystals. Journal of Physical Chemistry B. 2002;106:504–507. DOI: 10.1021/jp012040a.

[104] Ito A, Masumoto H, Goto T. Microstructure and electrical conductivity of $SrRuO_3$ thin films prepared by laser ablation. Materials Transactions. 2006;47(11):2808–2814.

[105] Pradier CM, Hinnen C, Jansson K, Dahl L, Nygren M, Flodstrom A. Structural and surface characterization of perovskite-type oxides; influence of A and B substitutions upon oxygen binding energy. Journal of Materials Science. 1998;33:3187–3191. DOI: 10.1023/A:1004312326617.

[106] Wu Q, Liu M, Jaegermann W. X-ray photoelectron spectroscopy of $La_{0.5}Sr_{0.5}MnO_3$. Materials Letters. 2005;59:1980–1983. DOI: 10.1016/j.matlet.2005.01.038.

[107] Ghasdi M, Alamdari H. CO sensitive nanocrystalline $LaCoO_3$ perovskite sensor prepared by high energy ball milling. Sensors and Actuators B. 2010;148:478–485. DOI: 10.1016/j.snb.2010.05.056.

[108] Ghasdi M, Alamdari H, Royer S, Adnot A. Electrical and CO gas sensing properties of nanostructured $La_{1-x}Ce_xCoO_3$ perovskite prepared by activated reactive synthesis. Sensors and Actuators B. 2011;156:147–155. DOI: 10.1016/j.snb.2011.04.003.

[109] Ru Z, Jifan H, Zhouxiang H, Ma Z, Zhanlei W, Yongjia Z, Hongwei Q. Electrical and CO-sensing properties of $NdFe_{1-x}Co_xO_3$ perovskite system. Journal of Rare Earths. 2010;28(4):591–595. DOI: 10.1016/S1002-0721(09)60160-5

[110] Fergus JW. Perovskite oxides for semiconductor-based gas sensors. Sensors and Actuators B. 2007;123:1169–1179. DOI: 10.1016/j.snb.2006.10.051.

[111] Song P, Wang Q, Yang Z. The effects of annealing temperature on the CO-sensing property of perovskite $La_{0.8}Pb_{0.2}Fe_{0.8}Cu_{0.2}O_3$ nanoparticles. Sensors and Actuators B. 2009;141:109–115. DOI: 10.1016/j.snb.2009.05.040.

[112] Doroftei C, Pop PD, Iacomi F. Synthesis of nanocrystalline La–Pb–Fe–O perovskite and methanol-sensing characteristics. Sensors and Actuators B. 2011;161(1):977–981. DOI: 10.1016/j.snb.2011.11.078

[113] Benali A, Azizi S, Bejar M, Dhahri E, Graça MFP. Structural, electrical and ethanol sensing properties of double-doping $LaFeO_3$ perovskite oxides. Ceramics International. 2014;40(9):14367–14373. DOI: 10.1016/j.ceramint.2014.06.029.

[114] Liu X, Cheng B, Hu J, Qin H, Jiang M. Semiconducting gas sensor for ethanol based on $LaMg_xFe_{1-x}O_3$ nanocrystals. Sensors and Actuators B. 2008;129:53–58. DOI: 10.1016/j.snb.2007.07.102.

[115] Wang Y, Chen J, Wu X. Preparation and gas-sensing properties of perovskite-type $SrFeO_3$ oxide. Materials Letters. 2001;49:361–364. DOI: 10.1016/S0167-577X(00)00400-6.

[116] Liu X, Hu J, Cheng B, Qin H, Jiang M. Preparation and gas sensing characteristics of p-type semiconducting $LnFe_{0.9}Mg_{0.1}O_3$ (Ln = Nd, Sm, Gd and Dy) materials. Current Applied Physics. 2009;9:613–617. DOI: 10.1016/j.cap.2008.05.014.

[117] Najjar H, Batis H. La–Mn perovskite-type oxide prepared by combustion method: Catalytic activity in ethanol oxidation. Applied Catalysis A: General. 2010;383:192–201. DOI: 10.1016/j.apcata.2010.05.048.

[118] Sun L, Qin HW, Cao E, Zhao M, Gao F, Hu J. Gas-sensing properties of perovskite $La_{0.}875Ba_{0.125}FeO_3$ nanocrystallinepowders. Journal of Physics and Chemistry of Solids. 2011;72:29–33. DOI: 10.1016/j.jpcs.2010.10.074.

[119] Kong L, Shen Y. Gas-sensing property and mechanism of $Ca_xLa_{1-x}FeO_3$ ceramics. Sensors and Actuators B. 1996;30:217–221. DOI: 10.1016/0925-4005(96)80052-9.

[120] Feng C, Ruan S, Li J, Zou B, Luo J, Chen W, Dong W, Wu F. Ethanol sensing properties of $LaCo_xFe_{1-x}O_3$ nanoparticles: effects of calcination temperature, Co-doping, and carbon nanotube-treatment. Sensors and Actuators B. 2011;155:232–238. DOI: 10.1016/j.snb.2010.11.053.

[121] Khetre SM. Ethanol gas sensing properties of nano-porous $LaFeO_3$ thick film. Sensors and Transducers. 2013;149(2):13–19.

[122] Zhang L, Hu J, Song P, Qin H, Jiang M. Electrical properties and ethanol-sensing characteristics of perovskite $La_{1-x}Pb_xFeO_3$. Sensors and Actuators B. 2006;114:836–840. DOI: 10.1016/j.snb.2005.08.002.

[123] Martinelli G, Carotta MC, Ferroni M, Sadaoka Y, Traversa E. Screen-printed perovskite-type thick films as gas sensors for environmental monitoring. Sensors and Actuators B. 1999;55:99–110. DOI: 10.1016/S0925-4005(99)00054-4.

[124] Carotta MC, Butturi MA, Martinelli G, Sadaoka Y, Nunziante P, Traversa E. Microstructural evolution of nanosized $LaFeO_3$ powders from the thermal decomposition of a cyano-complex for thick film gas sensors. Sensors and Actuators B. 1997;44:590–594. DOI: 10.1016/S0925-4005(97)00177-9.

[125] Di Bartolomeo E, Grilli ML, Yoon JW, Traversa E. NO_x sensors based on interfacing nano-sized $LaFeO_3$ perovskite-type oxide and ionic conductors. Project of Special Materials for Advanced Technologies—MSTA II. Via della Ricerca Scientifica, 00133 Rome, Italy.

[126] Sahner K, Moos R, Matam M, Tunney JJ, Post M. Hydrocarbon sensing with thick and thin film p-type conducting perovskite materials. Sensors and Actuators B. 2005;108:102–112. DOI: 10.1016/j.snb.2004.12.104.

[127] Giang HT, Duy HT, Ngan PQ, Thai GH, Thu DTA, Thu DT, Toan NN. Hydrocarbon gas sensing of nano-crystalline perovskite oxides $LnFeO_3$ (Ln = La, Nd and Sm). Sensors and Actuators B. 2011;158:246– 251. DOI: 10.1016/j.snb.2011.06.013.

[128] Jia F, Zhong H, Zhang W, Li X, Wanga G, Songa J, Cheng Z, Yin J, Guo L. A novel nonenzymatic ECL glucose sensor based on perovskite $LaTiO_3$-Ag0.1 nanomaterials. Sensors and Actuators B. 2015;212:174–182. DOI: 10.1016/j.snb.2015.02.011.

[129] Ye D, Xu Y, Luo L, Ding Y, Wang Y, Liu X, Xing L, Peng J. A novel nonenzymatic hydrogen peroxide sensor based on $LaNi_{0.5}Ti_{0.5}O_3/CoFe_2O_4$ modified electrode. Colloids and Surfaces B: Biointerfaces. 2012;89:10–14. DOI: 10.1016/j.colsurfb.2011.08.014.

[130] Zhang Z, Gu S, Ding Y, Jin J. A novel nonenzymatic sensor based on $LaNi_{0.6}Co_{0.4}O_3$ modified electrode for hydrogen peroxide and glucose. Analytica Chimica Acta. 2012;745:112–117. DOI: 10.1016/j.aca.2012.07.039.

[131] Luque GL, Ferreyra NF, Leyva AG, Rivas GA. Characterization of carbon paste electrodes modified with manganese based perovskites-type oxides from the amperometric determination of hydrogen peroxide. Sensors and Actuators B. 2009;142:331–336. DOI: 10.1016/j.snb.2009.07.038.

[132] Zhang Z, Gu S, Ding Y, Zhang F, Jin J. Determination of hydrogen peroxide and glucose using a novel sensor platform based on $Co_{0.4}Fe_{0.6}LaO_3$ nanoparticles. Microchim Acta. 2013;180:1043–1049. DOI: 10.1007/s00604-013-1012-9.

[133] Wang Y, Zhong H, Li X, Jia F, Shi Y, Zhang W, Cheng Z, Zhang L, Wang J. Perovskite $LaTiO_3$–Ag0.2 nanomaterials for nonenzymatic glucose sensor with high performance. Biosensors and Bioelectronics. 2013;48:56–60. DOI: 10.1016/j.bios.2013.03.081.

[134] Wang Y, Xu Y, Luo L, Ding Y, Liu X. Preparation of perovskite-type composite oxide $LaNi_{0.5}Ti_{0.5}O_3$–$NiFe_2O_4$ and its application in glucose biosensor. Journal of Electroanalytical Chemistry. 2010;642:35–40. DOI: 10.1016/j.jelechem.2010.02.001.

[135] Shimizu Y, Komatsu H, Michishita S, Miura N, Yamazo N. Sensing characteristics of hydrogen peroxide sensor using carbon based-electrode loaded with perovskite-type oxide. Sensors and Actuators B. 1996;34:493–498. DOI: 10.1016/S0925-4005(97)80021-4.

[136] Anh DTV, Olthuis W, Bergveld P. Sensing properties of perovskite oxide $La_{1-x}Sr_xCoO_{3-\delta}$ obtained by using pulsed laser deposition. MESA+ Research Institute, University of Twente: Enschede, The Netherlands. p. 618–620.

[137] El-Ads EH, Galal A, Atta NF. Electrochemistry of glucose at gold nanoparticles modified graphite/$SrPdO_3$ electrode—towards a novel non-enzymatic glucose sensor. Journal of Electroanalytical Chemistry. 2015;749:42–52. DOI: 10.1016/j.jelechem.2015.04.033.

[138] Wen CY. Study and Application of Composite Materials Based on Perovskite Nanoparticles [MSc thesis]. Jiangsu University of Science and Technology; 2011.

[139] Wang B, Gu S, Ding Y, Chu Y, Zhang Z, Ba X, Zhang Q, Li X. A novel route to prepare $LaNiO_3$ perovskite-type oxide nanofibers by electrospinning for glucose and hydrogen peroxide sensing. Analyst. 2013;138(1):362–367. DOI: 10.1039/c2an35989h.

[140] Thirumalairajan S, Girija K, Mastelaro VR, Ganesh V, Ponpandian N. Detection of the neurotransmitter dopamine by a glassy carbon electrode modified with self assembled perovskite $LaFeO_3$ microspheres made up of nanospheres. RSC Advances. 2014;4:25957–25962. DOI: 10.1039/C4RA03467H.

[141] Atta NF, Ali SM, El-Ads EH, Galal A. The electrochemistry and determination of some neurotransmitters at $SrPdO_3$ modified graphite electrode. Journal of the Electrochemical Society. 2013;160(7):G3144-G3151. DOI: 10.1149/2.022307jes.

[142] Thirumalairajan S, Girija K, Ganesh V, Mangalaraj D, Viswanathan C, Ponpandian N. Novel synthesis of $LaFeO_3$ nanostructure dendrites: a systematic investigation of growth mechanism, properties, and biosensing for highly selective determination of neurotransmitter compounds. Crystal Growth and Design. 2013;13:291–302. DOI: 10.1021/cg3014305

[143] Wang G, Sun J, Zhang W, Jiao S, Fang B. Simultaneous determination of dopamine, uric acid and ascorbic acid with $LaFeO_3$ nanoparticles modified electrode. Microchim Acta. 2009;164:357–362. DOI: 10.1007/s00604-008-0066-6.

[144] Haile SM. Fuel cell materials and components. Acta Materialia. 2003;51:5981–6000. DOI: 10.1016/j.actamat.2003.08.004.

[145] Shao Z, Haile SM. A high-performance cathode for the next generation of solid-oxide fuel cells. Nature. 2004;431:170–173. DOI: 10.1038/nature02863.

[146] Ding X, Kong X, Wang X, Jiang J, Cui C. Characterization and optimization of $Ln_{1.7}Sr_{0.3}CuO_4$ (Ln = La, Nd)-based cathodes for intermediate temperature solid oxide fuel cells. Journal of Alloys and Compounds. 2010;502:472–476. DOI: 10.1016/j.jallcom.2010.04.199.

[147] Song K, Lee K. Characterization of $Ba_{0.5}Sr_{0.5}M_{1-x}Fe_xO_{3-\delta}$ (M = Co and Cu) perovskite oxide cathode materials for intermediate temperature solid oxide fuel cells. Ceramics International. 2012;38:5123–5131. DOI: 10.1016/j.ceramint.2012.03.015.

[148] Conceição LD, Silva AM, Ribeiro NFP, Souza MMVM. Combustion synthesis of $La_{0.7}Sr_{0.3}Co_{0.5}Fe_{0.5}O_3$ (LSCF) porous materials for application as cathode in IT-SOFC. Materials Research Bulletin. 2011;46:308–314. DOI: 10.1016/j.materresbull.2010.10.009.

[149] Faro ML, Minutoli M, Monforte G, Antonucci V, Aricó AS. Glycerol oxidation in solid oxide fuel cells based on a Ni-perovskite electrocatalyst. Biomass and Bioenergy. 2011;35:1075–1084. DOI: 10.1016/j.biombioe.2010.11.018.

[150] Ling Y, Lin B, Zhao L, Zhang X, Yu J, Peng R, Meng G, Liu X. Layered perovskite $LaBaCuMO_{5+x}$ (M= Fe, Co) cathodes for intermediate-temperature protonic ceramic membrane fuel cells. Journal of Alloys and Compounds. 2010;493:252–255. DOI: 10.1016/j.jallcom.2009.12.072.

[151] Lianghao Y, Yonghong C, Qingwen G, Dong T, Xiaoyong L, Guangyao M, Bin L. Layered perovskite oxide $Y_{0.8}Ca_{0.}2BaCoFeO_{5+\delta}$ as a novel cathode material for inter-

mediate-temperature solid oxide fuel cells. Journal of Rare Earths. 2015;33(5):519–523. DOI: 10.1016/S1002-0721(14)60450-6.

[152] Chen Y, Wei Y, Zhong H, Gao J, Liu X, Meng G. Synthesis and electrical properties of $Ln_{0.6}Ca_{0.4}FeO_{3-\delta}$ (Ln Pr, Nd, Sm) as cathode materials for IT-SOFC. Ceramics International. 2007;33:1237–1241. DOI: 10.1016/j.ceramint.2006.03.035.

[153] Tongyun C, Liming S, Feng L, Weichang Z, Qianfeng Z, Xiangfeng C. $NdFeO_3$ as anode material for S/O_2 solid oxide fuel cells. 2012;30(11):1138–1141. DOI: 10.1016/S1002-0721(12)60194-X.

[154] Takahashl T, Iwahara H. Ionic conduction in perovskite-type oxide solid solution and its applications to the solid electrolyte fuel cell. Energy Conversion. 1971;11:105–111. DOI: 10.1016/0013-7480(71)90121-5.

[155] Bonanos N, Knight KS, Ellis B. Perovskite solid electrolytes: Structure, transport properties and fuel cell applications. Solid State Ionics. 1995;79:161–170. DOI: 10.1016/0167-2738(95)00056-C.

[156] Skinner SJ. Recent advances in perovskite-type materials for solid oxide fuel cell cathodes. International Journal of Inorganic Materials. 2001;3:113–121. DOI: 10.1016/S1466-6049(01)00004-6.

[157] Sun C, Stimming U. Recent anode advances in solid oxide fuel cells. Journal of Power Sources. 2007;171:247–260. DOI: 10.1016/j.jpowsour.2007.06.086.

[158] Wang F, Chen D, Shao Z. $Sm_{0.5}Sr_{0.5}CoO_{3-\delta}$-infiltrated cathodes for solid oxide fuel cells with improved oxygen reduction activity and stability. Journal of Power Sources. 2012;216:208–215. DOI: 10.1016/j.jpowsour.2012.05.068.

[159] Li H, Zhao Y, Wang Y, Li Y. $Sr_2Fe_{2-x}Mo_xO_{6-\delta}$ perovskite as an anode in a solid oxide fuel cell:Effect of the substitution ratio. Catalysis Today. DOI: 10.1016/j.cattod.2015.04.025.

[160] Raza MA, Rahman IZ, Beloshapkin S. Synthesis of nanoparticles of $La_{0.75}Sr_{0.25}Cr_{0.5}Mn_{0.5}O_{3-\delta}$ (LSCM) perovskite by solution combustion method for solid oxide fuel cell application. Journal of Alloys and Compounds. 2009;485:593–597. DOI: 10.1016/j.jallcom.2009.06.059.

[161] Huang YH, Dass RI, Xing ZL, Goodenough JB. Double perovskites as anode materials for solid-oxide fuel cells. Science. 2006;312:254–257. DOI: 10.1126/science.1125877

[162] Tao SW, Irvine JTS. A redox-stable efficient anode for solid-oxide fuel cells. Nature Materials. 2003;2:320–323. DOI: 10.1038/nmat871.

[163] Vernoux P, Guillodo M, Fouletier J, Hammou A. Alternative anode material for gradual methane reforming in solid oxide fuel cells. Solid State Ionics. 2000;135:425–431. DOI: 10.1016/S0167-2738(00)00390-8.

[164] Jin C, Cao X, Lu F, Yang Z, Yang R. Electrochemical study of $Ba_{0.5}Sr_0.5Co_{0.8}Fe_{0.2}O_3$ perovskite as bifunctional catalyst in alkaline media. International Journal of Hydrogen Energy. 2013;38:10389–10393. DOI: 10.1016/j.ijhydene.2013.06.047.

[165] Malkhandi S, Manohar AK, Yang B, Prakash GKS, Narayanan SR. Properties of calcium-doped lanthanum cobalt oxide perovskite electrocatalysts for oxygen evolution in alkaline medium. The Electrochemical Society. Abstract 292, 220th ECS Meeting. 2011.

[166] Kahoul A, Hammouche A, Nâamoune F, Chartier P, Poillerat G, Koenig JF. Solvent effect on synthesis of perovskite-type $La_{1-x}Ca_xCoO_3$ and their electrochemical properties for oxygen reactions. Materials Research Bulletin. 2000;35:1955–1966. DOI: 10.1016/S0025-5408(00)00395-0.

[167] Bao X, Wang Y, Zhu Q, Wang N, Zhu D, Wang J, Yang A, Yang R. Efficient planar perovskite solar cells with large fill factor and excellent stability. Journal of Power Sources. 2015;297:53–58. DOI: 10.1016/j.jpowsour.2015.07.081.

[168] Bhatt P, Pandey K, Yadav P, Tripathi B, KanthP C, Pandey MK, Kumar M. Investigating the charge carrier transport within the hole-transport material free perovskite solar cell processed in ambient air. Solar Energy Materials and Solar Cells. 2015;140:320–327. DOI: 10.1016/j.solmat.2015.04.028.

[169] Chen Q, Marco ND, Yang YM, Song T, Chen C, Zhao H, Hong Z, Zhou H, Yang Y. Under the spotlight: the organic-inorganic hybrid halide perovskite for optoelectronic applications. Nano Today. DOI: 10.1016/j.nantod.2015.04.009.

[170] Green MA, Ho-Baillie A, Snaith HJ. The emergence of perovskite solar cells. Nature Photonics. 2014;8:506–514. DOI: 10.1038/NPHOTON.2014.134.

[171] Park N. Perovskite solar cells: an emerging photovoltaic technology. Materials Today. DOI: 10.1016/j.mattod.2014.07.007.

[172] Schoonman J. Organic-inorganic lead halide perovskite solar cell materials: a possible stability problem. Chemical Physics Letters. DOI: 10.1016/j.cplett.2014.11.063.

[173] Sun H, Ruan P, Bao Z, Chen L, Zhou X. Shell-in-Shell TiO_2 hollow microspheres and optimized application in light-trapping perovskite solar cells. Solid State Sciences. 2015;40:60–66. DOI: 10.1016/j.solidstatesciences.2014.12.015.

[174] Tripathi B, Bhatt P, KanthP C, Yadav P, Desai B, Pandey MK, Kumar M. Temperature induced structural, electrical and optical changes in solution processed perovskite material: Application in photovoltaics. Solar Energy Materials and Solar Cells. 2015;132:615–622. DOI: 10.1016/j.solmat.2014.10.017.

[175] Wang X, Li Z, Xu W, Kulkarni SA, Batabyal SK, Zhang S, Cao A, Wong LH. TiO_2 nanotube arrays based flexible perovskite solar cells with transparent carbon nanotube electrode. Nano Energy. DOI: 10.1016/j.nanoen.2014.11.042.

[176] Werner J, Dubuis G, Walter A, Löper P, Moon S, Nicolay S, Morales-Masis M, Wolf SD, Niesen B, Ballif C. Solar Energy Materials and Solar Cells. 2015;141:407–413. DOI: 10.1016/j.solmat.2015.06.024.

[177] Yan W, Li Y, Li Y, Ye S, Liu Z, Wang S, Bian Z, Huang C. High-performance hybrid perovskite solar cells with open circuit voltage dependence on hole transporting materials. Nano Energy. DOI: 10.1016/j.nanoen.2015.07.024.

[178] Yang Z, Cai B, Zhou B, Yao T, Yu W, Liu FS, Zhang W, Li C. An up-scalable approach to $CH_3NH_3PbI_3$ compact films for high-performance perovskite solar cells. Nano Energy. DOI: 10.1016/j.nanoen.2015.05.027.

[179] Yeo J, Kang R, Lee S, Jeon Y, Myoung N, Lee C, Kim D, Yun J, Seo Y, Kim S, Na S. Highly efficient and stable planar perovskite solar cells with reduced graphene oxide nanosheets as electrode interlayer. Nano Energy. DOI: 10.1016/j.nanoen.2014.12.022.

IntechOpen